NUMERICAL SIMULATION OF FLOW AND HEAT TRANSFER IN INTERNAL MULTI-PASS COOLING CHANNEL WITHIN GAS TURBINE BLADE

A Thesis

by

HUNG-CHIEH CHU

Submitted to the Office of Graduate Studies of
Texas A&M University
in partial fulfillment of the requirements for the degree of

MASTER OF SCIENCE

Approved by:

Co-Chairs of Committee,	Je-Chin Han
	Hamn-Ching Chen
Committee Member,	Gerald Lee Morrison
Head of Department,	Jerald A. Caton

December 2012

Major Subject: Mechanical Engineering

ABSTRACT

Results from numerical simulation were performed to study flow and heat transfer in two types of rotating multi-pass cooling channels. Second moment closure model was used to solve flow in domain generated from Chimera method.

The first type was a four-pass channel with two different inlet settings. The main flowing channel was rectangular channel (AR=2:1) with hydraulic diameter (D_h) equals to 2/3 inch (16.9 mm). The first and fourth channel were set as different aspect ratio (AR=2:1; AR=1:1). Reynolds number (Re) used in this part was 10,000. The rotating angle was set as 90 degrees. The density ratio was set as 0.115. The rotation number varied from 0.0 to 0.22. It was showed that inlet effect only caused influence to flow and heat transfer in first two passages.

The second type was a four-pass channel with/without addition of vane in smooth turn portion. The main flowing channel was rectangular channel (AR=2:1) with hydraulic diameter (D_h) equals to 2/3 inch. The first and fourth passages were set to be square duct (AR=1:1). The Reynolds number (Re) used in this part was 20,000. Three rotation numbers were set here (Ro=0.0; Ro=0.2; Ro=0.4). The density ratio and rotating angle varied from 0.12 to 0.32 and from 45 degrees to 90 degrees respectively. According to numerical results, it was revealed that the addition of vane in smooth turn portion did not cause influence to part before it. However, it caused significant influence to flow and heat transfer in smooth turn portion and part after it.

ACKNOWLEDGEMENTS

I would like to express my appreciation to my two advisors, Dr. Je-Chin Han and Dr. Hamn-Ching Chen, for their patience and guidance. Without their help, I could not finish my thesis. I also appreciate my academic committee member; Dr. Gerrald Lee Morrison. Thanks for his precious time and helpful suggestions.

Thanks also go to Mr. Shang-Feng Yang and Mr. Sam Wu, who are my colleagues from the Turbine Heat Laboratory. Discussions with them always help me to clarify my mind.

Finally, I am most grateful to my parents and my wife for their support and encouragement. Since their sacrifice, I could finish this thesis.

The computations were performed on the EOS supercomputer system at the Texas A&M Supercomputer Center under a supercomputer research grant. I am grateful for this this support.

NOMENCLATURE

D_h	hydraulic diameter
h	heat transfer coefficient
k	thermal conductivity of coolant
L	length of the duct
Nu	local Nusselt number
Nu_o	Dittus-Boelter correlation
Pr	Prandtl number
Re	Reynolds number
Ro	rotation number
T	local temperature
Tc	inlet coolant temperature
Tw	wall temperature
ρ	density of coolant
$\Delta\rho/\rho$	coolant-to-wall density ratio
Ω	rotation speed
θ	dimensionless temperature

TABLE OF CONTENTS

Page

LIST OF FIGURES

Page

LIST OF TABLES

Page

CHAPTER I

INTRODUCTION AND LITERATURE REVIEW

Gas turbine is equipment which has been widely used in industry, like aircraft engine and power plant electricity generation. Basic mechanism of it is to inject high temperature gas from combustor to rotate turbine blade, it changes energy form from thermal energy to mechanical energy. In order to get high efficiency, engineers try to increase inlet gas temperature. However, it is contradictory that the increase of high temperature will devastate turbine blade, since it is far above the allowable temperature of the material used in turbine blade manufacturing. It is necessary for people to figure out effective cooling mechanisms to protect turbine blade. With the goal of solving this problem, there are many cooling technologies invented, such as film cooling and impingement cooling. Among these technologies, internal cooling is one common method, which has high efficiency.

Internal cooling is to use an air compressor to inject cooling air into flowing channel within turbine blade to cool down high surface temperature of turbine blades. To an engineer, it is a big issue to design this cooling channel, since its irregular shape and limited space. Mostly, the flowing channel is a serpentine passage composed of several straight ducts and 180 degree sharp/smooth turns.

Turn play an important role in this multi-pass channel, it changes flow direction, causes important influence to flowing field and heat transfer. Sometimes, for the purpose to enhance heat transfer, engineers put turbulators in straight duct of internal cooling

channel, such as ribs with different angles, vanes and dimples. These turbulators induce secondary flow and generate many vortices which increase complexities of flowing field.

In reality, turbine blade rotates at very high rotating speed. Compared to non-rotating channel, rotation induces Coriolis force and buoyancy force, which cause significant influence to flowing field and local heat transfer.

The broad use of gas turbine in industrial applications makes internal cooling important. It is important for engineers/scientists to do research to get more detailed information about flow and heat transfer in the internal coolant passage. Several topics will be studied in this research. The related literature will be mentioned in the literature review.

1.1 Literature Review

1.1.1 Turn Effect

The small volume within turbine blade confines the size of internal flowing channel. In order to effectively use coolant to get good efficiency, the internal cooling passage is usually a multi-pass channel with several turn portions. In this kind of geometry, turn becomes an important part, since it changes flow direction, cause flow attachment and change heat transfer. These effects are so-called turn effects.

Ekkad and Han [1] used liquid crystal transient technique to investigate heat transfer distribution in two-pass square channels with 180 degree sharp turn. They coated liquid crystal on the surface of turbine blade since liquid crystal changes with

temperature; this method can grab surface temperature variation efficiently. According to their data, it was showed that Nusselt number ratio (Nu/Nuo) in second passage is nearly 2-3 times higher than it is in first passage due to the turn effect.

Liou and Chen [2] did experiment by the use of Laser Doppler Velocimetry (LDV) to measure heat transfer in a two–pass smooth passage with a 180° rectangular sharp turn. They conclude that to a non-rotating channel, the secondary flow induced by the sharp turn is one of the main reasons to cause heat transfer enhancement in the portion after turn.

In Luo and Razinsky [3], four different turbulence models (V2F, k-ε model, shear stress transport (SST), Reynolds Stress model (RSM)) were used to predict flow in a U-duct. There were two types of turn used in their researches, one is turn with sharp corner (sharp turn) and the other is turn with round corner (smooth turn). Their results showed that compared to sharp turn, smooth turn decreased secondary flow in turn portion and the beginning potion after turn. This was one of the reasons which caused a substantial reduction in pressure loss in the turn portion.

1.1.2 Vane Effect

The complicated geometries of internal passage cannot avoid high pressure loss, especially to turn portions in a multi-pass channel. Strong secondary flow and flow separation occur here. These are the main reasons to cause high pressure loss in this portion. Engineers try to add a guide vane in the turn portion to decrease the loss.

According to numerical simulation did by Luo and Razinsky [3], the application of vane could reduce 38% Secondary-flow kinetic energy (SKE), which is a main reason to cause pressure loss. The combination of vane and turn with round corner could reduce more than 73%.

Zehnder et al. [4] add vanes at different positions in a two-pass ribbed channel to see its influence. Except doing experiment, they also used three different turbulence models (the reliable k-ε model with two-layer wall treatment, the k-ω –SST model, and the v^2-f turbulence model) to do comparison. Their experiment results showed that with the suitable design, the application of vane in turn portion can reduce pressure loss by about 25% and keep heat transfer level high. However, with inappropriate setting, the pressure loss would be increased by about 12% instead, accompanied with heat transfer decrease. As to their numerical simulation, they concluded that the results gained from the reliable k-ε model always showed under-prediction in pressure loss and heat transfer, in contrast, v2-f turbulence model showed over-prediction in heat transfer. Compare to the other two models, k-ω –SST model was the best choice to do this calculation, even it still showed 10-20 % over-prediction in heat transfer.

Chen et al. [5] used liquid crystal method to investigate vane effects in a ribbed two-pass square channel. In order to get detailed understanding, three different turbulence models were be used in their research, such as k-ε model, the SST reattachment model and Omega Reynolds Stress turbulence model (ORS). They concluded that this guide vane did not cause big influence to first passage (before turn); however, it indeed caused significant influence to turn portion and second passage (after

turn). They also mentioned that with suitable arrangement, vane can meet the requirement on heat transfer and pressure drop. As to their simulation, the numerical results all showed over-prediction in heat transfer. Among the three models, they thought ORS model was the better choice, although it still over-predicted by about 15%~35%.

1.1.3 Rotation Effect

In real engineering application, turbine blades rotate with high rotating speed. Compared to non-rotating channel, Coriolis force and Buoyancy force induced by rotation change flowing field within channels and also have significant influence to local heat transfer. Since its importance, there were many researchers studied this topic.

Wagner and Velkoff [6] used a rotating duct to study secondary flows in a rotating duct. They measured velocities and pressures at different positions within rotating duct and got the conclusion that magnitude of the cross-flow velocities and longitudinal vortices are linearly proportional to the rotational speed.

Dutta and Han [7] studied heat transfer in rotating smooth and ribbed two-pass square channels by the use of thermocouples. In their research, dimensionless parameter Nu/Nuo was used to judge heat transfer enhancement. To radially outward flow (from hub to tip), their experiment data showed that rotation enhanced heat transfer on trailing surface but decreased heat transfer on leading surface. However, to radially inward flow, rotation caused opposite effects.

Huh et al. [8] set different rotating speed (0-400RPM) to see rotation effects on heat transfer in a two-pass rectangular (AR=2:1) channel. They concluded that with high rotation, heat transfer could greatly be increased to Nu/Nuo=4.5 in the turn portion.

Hwang and Lai [9] used laminar flow model to simulate flow in a rotating multi-pass square channel. In order to keep the flow state still in laminar flow, the Reynolds number they set were all under 2000. Although their settings were limited, their simulation still gave basic understandings about vortices and temperature distribution in the cooling channel.

To precisely simulate flow in internal flowing channel, turbulent models are needed, such as RANS models and LES models. Saha and Acharya [10] used RANS model to simulate turbulent flow and heat transfer in ribbed coolant passage of different aspect ratios (AR=1:1, 4:1 and 1:4). Their results revealed that the increase of rotation number increases heat transfer on all confining walls, except the trailing wall in 1:4 AR duct. They also mentioned that friction factor increases with the increase of rotation number.

Chen et al. [11] used second moment closure model to simulate flow and heat transfer in multi-pass cooling channels and compared their results to experiment data in Wagner et al. [12]. No matter in non-rotating or rotating condition, their results always showed good agreement with experiment data. Besides, since it also solved near wall region, it was cleared to see the anisotropy of flow.

Su et al. [13] Calculated flow and heat transfer in rotating two-pass smooth channel with different aspect ratio (AR=1:1, 1:2 and 1:4) by the use of second moment

closure model. According to their simulation, secondary flow induced by rotation changed the range and strength of vortices on cross section. This reasonably resulted in changes of local heat transfer. The numerical results also showed good agreement with experiment data in Fu et al. [2004].

Tyagi and Acharya [14] used LES to predict flow and heat transfer in rotating ribbed duct flows. Their results clearly showed that LES can capture physic phenomenon of turbulent flow within rotating ribbed duct.

1.1.4 Density Ratio Effect

To internal cooling channel, lower temperature theoretically can get better efficiency**.** Inlet density ratio ($\Delta\rho/\rho$) has been widely used in this research.

Wagner et al. [12, 15] measure heat transfer in a rotating multi-pass channel by the set of four-pass square channel. In their experiment, different density ratios ($\Delta\rho/\rho$=0.07~0.22) were set to see its effect. According to their experiment data, higher density ratio got good heat transfer. However, on the leading side near the inlet, heat transfer decreased with the increase of density ration. They thought the decreases were resulted by both the interaction of the near–wall flow stability and the buoyance effects. The numerical results in Chen et al [16] also showed similar results in Wagner et al. [15].

1.1.5 Inlet Effect

Wright et al. [17] set three different entrance conditions (fully developed, sudden contraction, and partial sudden contraction) to investigate entrance effect. The concluded that entrance geometry has a significant effect on the heat transfer in rotating/non-rotating smooth channels. However, the entrance effect will be decreased with the increase of rotation number.

1.2 Research Objectives

The main method in this research is to investigate flow and heat transfer in internal multi-pass cooling channels by the use of second moment closure model. Two topics will be studied:

1. Inlet effect: The first passage of the four-pass channel will be set as different aspect ratio (AR=2:1; AR=1:1) to investigate influence from different inlet settings.
2. Vane effect: Previous literatures related to vane were all under non-rotating condition. It is deficient for practical use. In this research, second moment closure model will be used to predict flow and heat transfer in a multi-pass rectangular (AR=2:1) channel with application of a guide vane in smooth turn. Several topics will be discussed. Numerical results will be compared to experiment data in Lei et al. [18] to get detailed analysis.

CHAPTER II

GOVERNING EQUATION AND GRID GENERATION

There are several methods used to solve turbulent flow main method in this research is to investigate flow and heat transfer in internal multi-pass cooling channels by the use of second moment closure model.

(1) LES method: The basic concept is to use space-average to divide flow into two parts. It assumes that more than 90% of flow properties are solved directly by Navier-Stokes equations, only less 10% flow properties are solved by models. Tyagi and Acharya [14] used this method to simulate flow and heat transfer in rotating ribbed duct flows. The results showed that this method can get very detailed information about flow in this duct. However, there is a big disadvantage in this method. In order solve 90 % turbulent flow directly; the grid size has to be small enough. It will spend a lot of time and computer resource, since this strictly criteria.

(2) DNS method: It solves all the physical properties directly without any model. It has been viewed as the most accurate numerical method to deal with turbulent flow. However, the grid size should be small enough to catch all physical phenomena. It needs large computer resource to do this calculation.

(3) RANS method: The basic concept of it is to use time average to divide physical properties into average terms and fluctuation term. Assumption will be made to solve fluctuation terms. Unlike previous two methods, the request to grid size is

much flexible; this saves time and makes it more applicable in engineering use. Most commercial codes put large amount of source on RANS models developing. There are several models belong to this model, such as k-ε model, k-ω model and Reynolds Stress model (RS).

In the present study, calculations were performed by the second moment closure model. This model belongs to RANS model and was originally developed by Chen [19] [20] to deal with non-rotating incompressible flow. It combined two RANS model, two-layer k-ε model and near-wall Reynolds Stress model. To make it more applicable in flow and heat transfer in rotating channel calculation, Chen et al. [11] [16] modified it.

2.1 Governing Equation of Second Moment Closure Model

For unsteady, incompressible, rotating flow, Reynolds stress model can be expressed as:

$$\frac{\partial \rho}{\partial t} + (\rho U^i)_{,i} = 0 \tag{2- 1}$$

$$\rho(\frac{\partial U^i}{\partial t} + U^m U^i_{,m} + R^{im}_{,m}) + 2\rho g^{il} e_{lmn} \Omega^m U^n + \rho g_{mn}(\Omega^i \Omega^m \xi^n - \Omega^m \Omega^n \xi^i) = -g^{im} p_{,m} + \mu(g^{mn} U^i_{,n})_{,m} \tag{2- 2}$$

Here, Reynolds stress transport equation has to be involved to solve Reynolds stress terms $R^{ij} = \overline{u^i u^j}$ occurred in momentum equations.

$$\frac{\partial R^{ij}}{\partial t} + U^m R^{ij}_{,m} = P^{ij} + D^{ij}_u + D^{ij}_p + D^{ij}_v + \Phi^{ij} - \varepsilon^{ij} \tag{2- 3}$$

Where P^{ij}, D^{ij}_u, D^{ij}_p, D^{ij}_v, Φ^{ij}_u, and ε^{ij} represent the production term, diffusion term by velocity fluctuation, diffusion term by pressure fluctuation, diffusion term by viscous, pressure strain term and viscous dissipation term.

In turbulent flow, how to deal with near wall region is always a critical issue. Unlike fully turbulent region, flow in this region is more close to laminar flow due to viscous effect. Some experts used wall function to do turbulent flow calculation. Instead of solving near wall region, it assumes that the first nearest points lies on fully turbulent region and obeys the logarithmic law. With this, all the physical properties can be obtained. The use of wall function can get solutions quickly due to the saving of grid number in near wall region. This method has been widely used in commercial code, such as Fluent, CFX and Star CD. However, accuracy may be lost when there is strong curvature in flowing channel. As to near-wall Reynolds stress model used here, whole flowing domain will be divided into two regions: near wall region and fully turbulent region. All regions will be solved directly by Eq. (2-1) ~Eq. (2-3).

It is well known that Reynolds Stress model is the most accurate model among RANS models since it solves Reynolds stress individually. Nevertheless, it is hard to use it directly because there are too many unknowns in it. To solve this problem, in the second moment closure model, two-layer k-ε model will be used prior to the use of near-wall Reynolds Stress model.

The hardness of solving Reynolds stress terms cause experts to develop turbulent-viscosity model. The basic concept is to use turbulent viscosity to get Reynolds stress, instead of solving them individually. Reynolds stress terms can be expressed as:

$$-\rho R^{ij} = 2\mu_t S^{ij} - \frac{2}{3} g^{ij} \rho k \qquad (2\text{-}4)$$

Where $k = g^{ij}\overline{u^i u^j}/2$ is turbulent kinetic energy.

Two-layer k-ε model was developed by Chen and Patel [21] to calculate two-dimensional turbulent wake flow. Chen et al. [22] expanded it to three-dimensional incompressible flow. In this model, whole flowing domain is also divided into near wall region and fully turbulent region. In the fully turbulent region, turbulent kinetic energy transport equation and dissipation energy transport equation will be used to calculate turbulent viscosity:

$$\rho(\frac{\partial k}{\partial t}+U^i k_{,i}) = g^{ij}\{(\mu+\frac{\mu_t}{\sigma_k})k_{,j}\}_{,i} + P + P_b - \rho\varepsilon \tag{2- 5}$$

$$\rho(\frac{\partial \varepsilon}{\partial t}+U^i \varepsilon_{,i}) = g^{ij}\{(\mu+\frac{\mu_t}{\sigma_\varepsilon})\varepsilon_{,j}\}_{,i} + \frac{\varepsilon}{k}(C_{\varepsilon 1}P + C_{\varepsilon 3}P_b - C_{\varepsilon 2}\rho\varepsilon) \tag{2- 6}$$

Where

$$P = 2g_{jm}\mu_t S^{ij}U^m_{,i} \tag{2- 7}$$

$$P_b = \frac{\mu_t}{\mathrm{Pr}_t} g^{ij}(\Omega^i\Omega^l\xi^j - \Omega^i\Omega^j\xi^l)T_{,l} \tag{2- 8}$$

In the near wall region, only k transport equation is needed, since dissipation energy will be expressed as function of k:

$$\varepsilon = \frac{k^{\frac{3}{2}}}{l_\varepsilon} \tag{2- 9}$$

$$l_\varepsilon = C_l y[1-\exp(-R_y / A_\varepsilon)] \tag{2- 10}$$

$$R_y = \sqrt{ky}/\nu \tag{2- 11}$$

The solutions gained from two-layer k-ε model will be used as the initial conditions to near-wall Reynolds Stress model. With these treatments, the false

assumption of in k-ε model can be corrected in near-wall Reynolds stress model. To Near-wall Reynolds stress model, it can be run without too many unreasonable assumptions.

In order to evaluate heat transfer energy transport equation will be induced to solve temperature field:

$$\rho C_p[\frac{\partial T}{\partial t}+U^i T_{,i}+(\overline{u^i T'})_{,i}]=g^{ij}(KT_{,j})_{,i}+\frac{Dp}{Dt}+\Phi \qquad (2\text{-}12)$$

Since Mach number is quite low, the flow will be considered as incompressible flow. Although the set is incompressible, density still has slightly variation due to the temperature difference. In this research, $\rho=\rho_o T_o/T$ will be used to deal with this, where ρ_o and T_o are inlet density and inlet temperature at the inlet of the channel.

2.2 Grid Generation

To CFD, engineer may spend a lot of time in grid generation, especially when there is strong curvature in geometry. To generate grid which match-up the shape, engineers usually divide whole domain into several parts and generate grid individually. In this situation, how to successfully transfer value from one block to its neighboring block becomes a big issue challenge. In this research, Chimera method will be used in grid establishment.

It is an open source code which was invented by NASA. According to Benek et al. [23] [24], the basic concept of it is to create an overlapped region between two neighboring blocks. In this region, interpolation will be used to renew boundary values

of each block. It offers engineers more freedom to generate grid. However, a possible deficiency of this method is it may lose mass. To make it more applicable for practical use, Hubbard and Chen [25] modified it to make sure during the calculation procedure, the flow still can reach mass conservation.

The configurations in this research were draw by the use of SolidWorks 2011. The commercial code GRIDGEN was used to generate Chimera grid. Since near wall region will be a key issue in this research, in order to get detailed information about this region, distance from boundary to nearest point should be small enough to keep y+ less than 0.5. According to the Reynolds number used in this research, for Re=10,000, the distance will be set as 0.0005 hydraulic diameter, for Re=20,000, 0.00025 hydraulic diameter will be set as the distance between boundary and its nearest point.

CHAPTER III

FLOW AND HEAT TRANSFER IN MULTI-PASS SMOOTH CHANNEL WITH DIFFERENT INLET

The main objective of the chapter is to predict inlet effect on flow and heat transfer in a four-pass cooling channel by the use of second moment closure model.

3.1 Description of Geometry and Computation Grid

There are three geometries used in this chapter, the first one is a two-pass rectangular (AR=2) channel. In Mohammad [26], the numerical results gained from this geometry had been compared to experiment data in Azad et al. [27]. In order to get fully-developed flow, there is an extension in first passage. The other two geometries are all four-pass channels. The second and third passage are both rectangular ducts with same aspect ratio (AR=2:1). However, the first and the fourth passage are set with different aspect ratio (AR=2:1, 1:1). The entrance will be extended, like it in Mohammad's. In these four-pass channels, first and second passage will be connected by a sharp turn, same arrangement will be set in connection between third and fourth passage. The second and third channels are connected by a smooth turn.

Fig. 3.1 is concept geometry of two-pass and four-pass cooling channel. To unify the measure standard, the hydraulic diameter used here is calculated from the dimension of two-pass rectangular channel and dimension of second and third passage in four-pass channel. The aspect ratio of these parts are all AR=2:1, which result in hydraulic

diameter, Dh= 16.9mm. The rotating angle in this chapter is 90°, which is the angle measured from the angle between rotating axis (+y axis) and direction of rotation (+x axis). The distance between the rotating axis and entrance, Rr/Dh, is 20.00. In two-pass channel or four-pass channels, they all include non- heating part in first passage. The length of non-heating part is given as Le/Dh=12.84. The distance from an entrance to the bottom of flowing channel is given as L/Dh=22.15, which is the summation of length of non-heating part, Le and length of heating part, L_h.

The grid used in two-pass channel is based on Mohammad's dissertation; there are 41×33 grid points on cross section and 125 grid points on streamwise direction.

Fig. 3.2 is the grid independent test for four-pass channel used in this research. Three grid sets were used to do grid independent test: (1) Grid 1, with 41×33 on cross section and 263 on streamwise direction. (2) Grid 2, 41×33 on cross section and 501 on streamwise direction. (3) Grid 3, 61×49 on cross section and 263 on streamwise direction. According to these results, in this research, the grid points used in cross section are 41×33. As to stream-wise direction, 263 grid points are used in four-pass channel. In order to get detailed information about near wall region, the distance from boundary to nearest points should be small enough to keep y+ less than 0.5. For cases with Re=10k, the distance from boundary to nearest point is 0.0005 of hydraulic diameter.

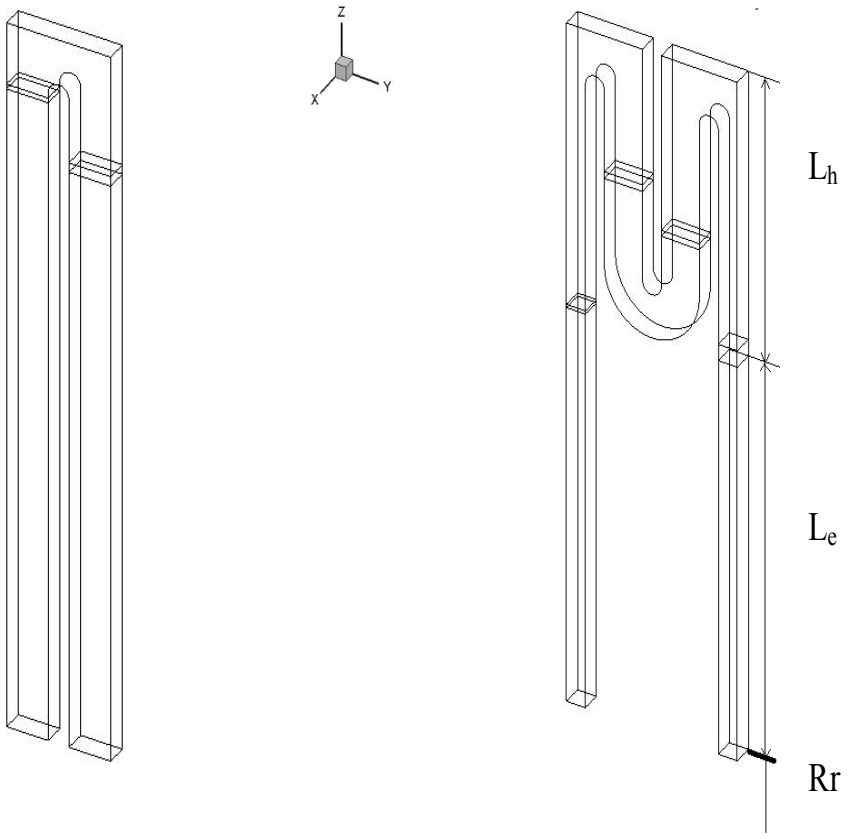

(a) Two-pass rectangular channel (b) Four-pass channel with different inlet

Fig. 3.1 Geometry of two-pass and four-pass cooling

Case No.	Re	$\Delta\rho/\rho$	Ro	β	Remark
1	10,000	0.115	0.0	-	Two-pass, aspect ratio is 2:1
2	10,000	0.115	0.0	-	Four-Pass, aspect ratio of whole flowing channel is 2:1
3	10,000	0.115	0.11	90	Four-Pass, aspect ratio of whole flowing channel is 2:1
4	10,000	0.115	0.22	90	Four-Pass, aspect ratio of whole flowing channel is 2:1
5	10,000	0.115	0.0	-	Four-Pass, aspect ratio of first and fourth pass is 1:1
6	10,000	0.115	0.11	90	Four-Pass, aspect ratio of first and fourth pass is 1:1
7	10,000	0.115	0.22	90	Four-Pass, aspect ratio of first and fourth pass is 1:1

Table 3.1 Summary of cases studied for inlet effect

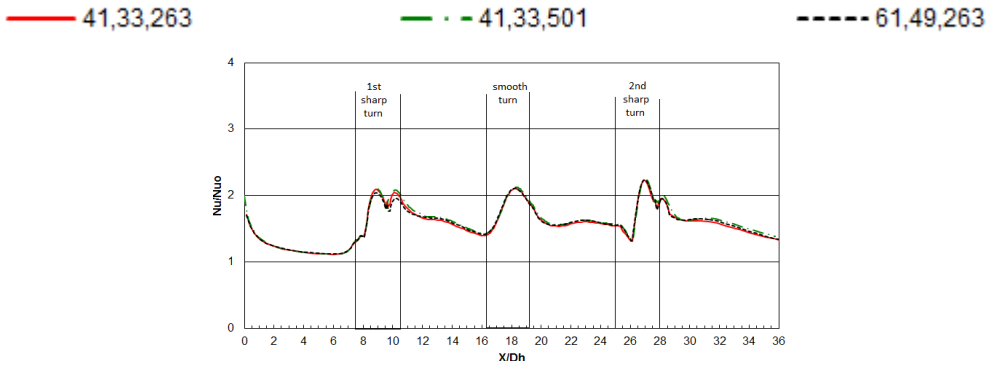

(a) Leading surface

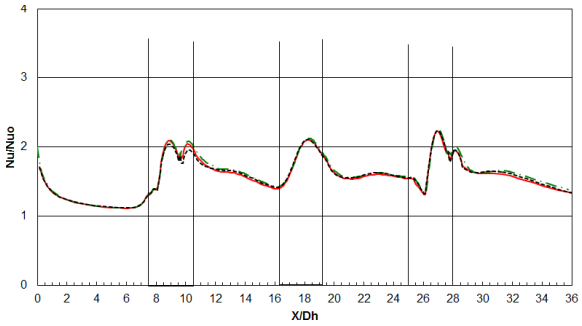

(b) Trailing surface

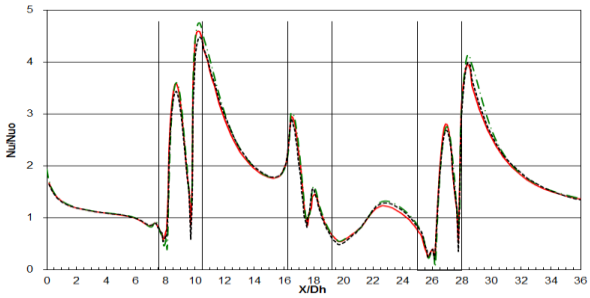

(c) Inner surface

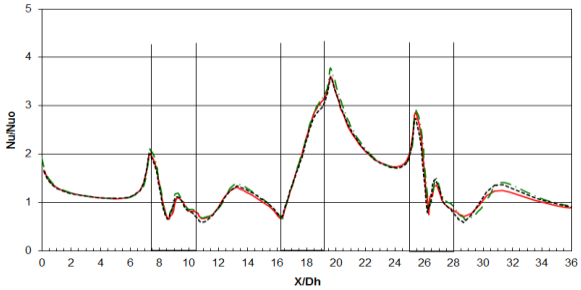

(d) outer surface

Fig. 3.2 Grid independent test

3.2 Case Study

Table 3.1 shows the summary of cases studied in this chapter. There are seven cases used here with fixed Reynolds number, Re is equal to 10k and inlet density ratio, $\Delta\rho/\rho$, equals to 0.115. Rotating angle is 90 degree. Rotation speed will be set from 0.0~0.22 to see rotating effect

3.3 Computation between Two-Pass Channel and Four-Pass Channel

Numerical results gained from four-pass rectangular (AR=2:1) channel will be compared to numerical results gained from two-pass channel in this part. Since the heating part is what we want, these parts will be output specially to do detailed description.

3.3.1 Velocity and Temperature Field

Fig. 3.3 is the velocity field and temperature distribution at the center part of cooling channels. Results gained from Case 1 shows turn effect causes flow attachment in the outer wall region at the beginning part of second passage. It also causes reverse flow and high temperature in the inner wall region. Compared to Case 1, flow in the first two passages of Case 2 shows almost identical behaviors.

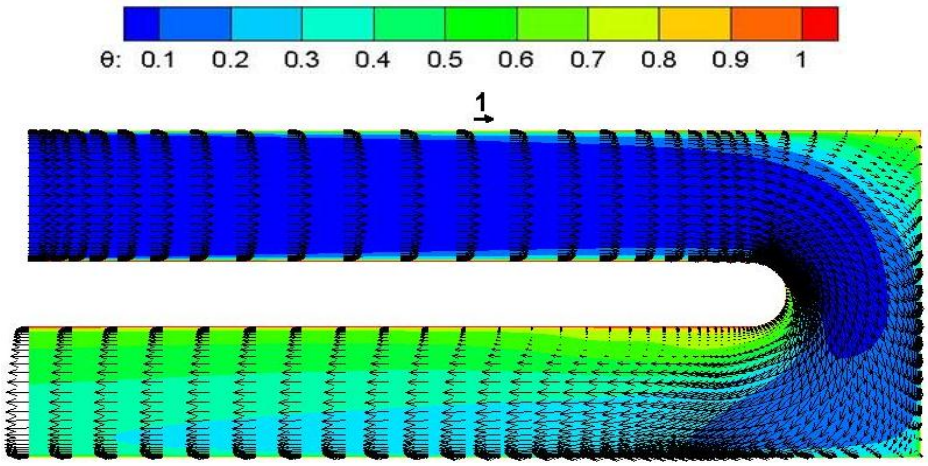

(a) Case 1: Ro=0.0, Two-Pass

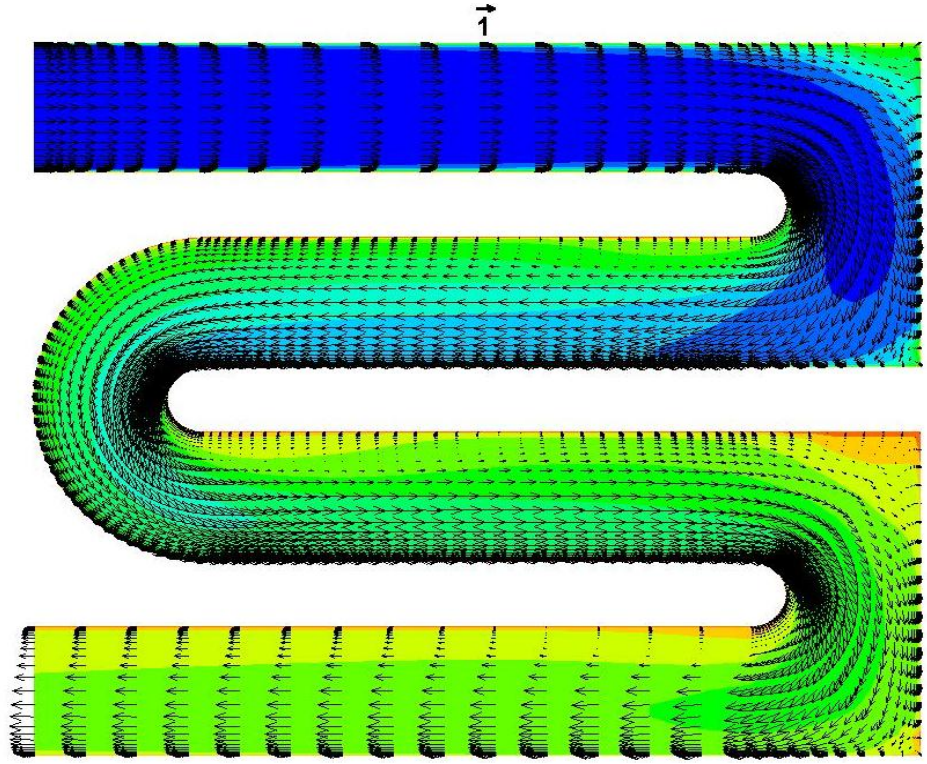

(b) Case 2: Ro=0.0, Four-Pass

Fig. 3.3 Velocity vector and temperature distribution of two-pass and four-pass rectangular (AR=2:1) channel

3.3.2 Heat Transfer

Nusselt number ratio, Nu/Nu0, will be used here to evaluate heat transfer enhancement. Nu_0 is Dittus-Boelter correlation, which is for fully developed turbulent non-rotating tube flow. It can be expressed as:

$$Nu_0 = 0.023\,\mathrm{Re}^{0.8}\,\mathrm{Pr}^{0.4} \qquad (3\text{-}1)$$

If Nu/Nu_0 is larger than 1, that means heat transfer enhancement. In this portion numerical result will also be compared to experiment data in Azad et al. [25].

Fig. 3.4 shows spanwise-averaged Nusselt number ratio for non-rotating two-pass and four-pass channels. On leading and trailing surface, results from Case 1 and Case 2 are almost identical, regardless of the trend or values. Comparison between numerical results and experiment data shows that numerical results have good agreement with experiment data. On inner surface, two numerical results are also identical. The big difference between numerical results and experiment results is on the outer surface of first passage. Results from Case 1 and 2 under-predict heat transfer in this region. However, in first sharp turn and second passage, numerical results shows good agreement with experiment data.

According to the results mentioned above, it can be concluded that flow in the first two passages of this four-pass channel shows similar behaviors as it in two-pass channel. Second moment closure model can successfully give detailed information about flow and heat transfer within it.

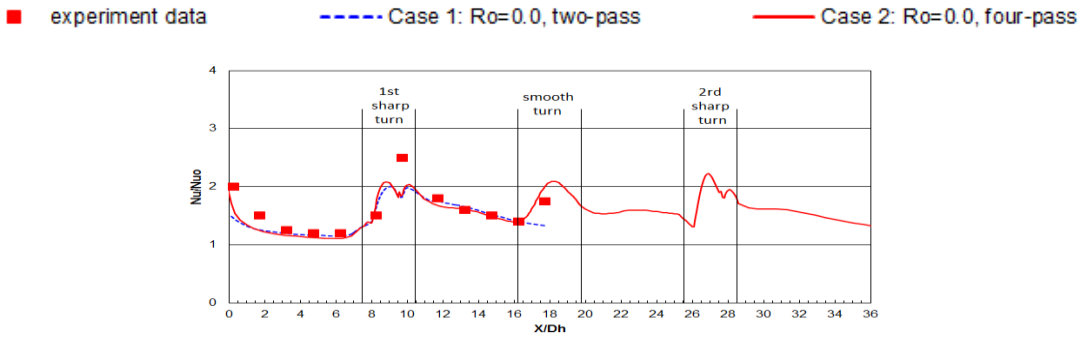

(a) Leading Surface

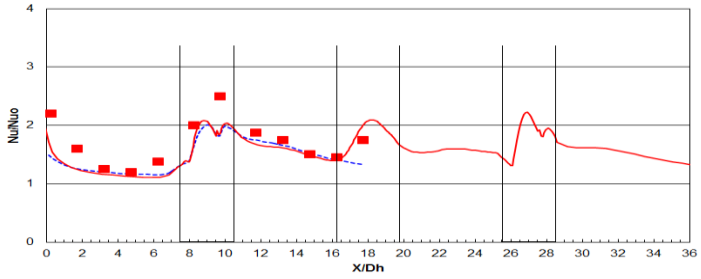

(b) Trailing Surface

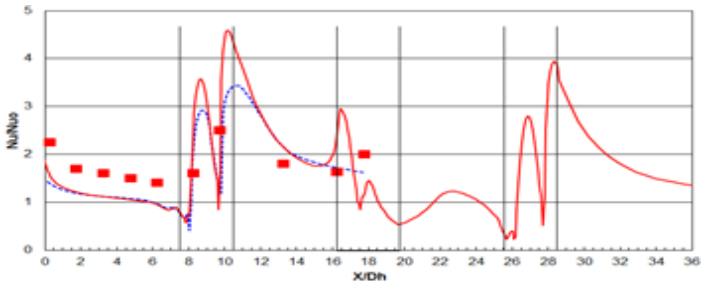

(c) Inner Surface

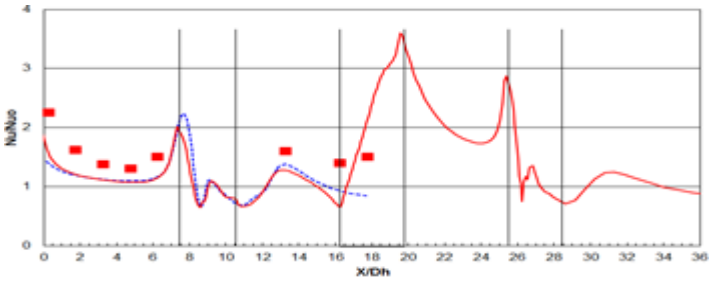

(d) Outer Surface

Fig. 3.4 Spanwise-averaged Nusselt number ratio from different channels

3.4 Prediction of Flow and Heat Transfer in Four-Pass Channel with Different Inlet

Second moment closure model will be used to give predictions to four-pass channel with different inlet. In this part, first passage will be set as different aspect ratio (AR=2:1, 1:1) and for symmetric geometry, same arrangement will be set in fourth passage.

3.4.1 Velocity and Temperature Field

Fig. 3.5 shows velocity vector and temperature distribution at the center portion of non-rotating flowing channels with different inlet settings. Results from Case 2 shows that flow impinges outer wall in the first shape turn. Since turn effect, flow attachment occurs in the beginning part of second passage and cause reverse flow area on its opposite side. Flow attachment occurs again in the inner region of smooth turn, since turn effect from smooth turn. This also cause flow attachment and reverse flow region in third passage. Similar behaviors occur in the second sharp turn and fourth passage. Compared to results from Case 2 and Case 5, it is clear to see that with fixed mass flow rate, the decrease of aspect ratio will increase inlet velocity in first passage. Since stronger flow impinges outer surface, the area of reverse flow becomes larger. In smooth turn and parts after it, two cases show similar results. This means this inlet effect only causes significant influence to first and second passage when the channel is under non-rotating condition.

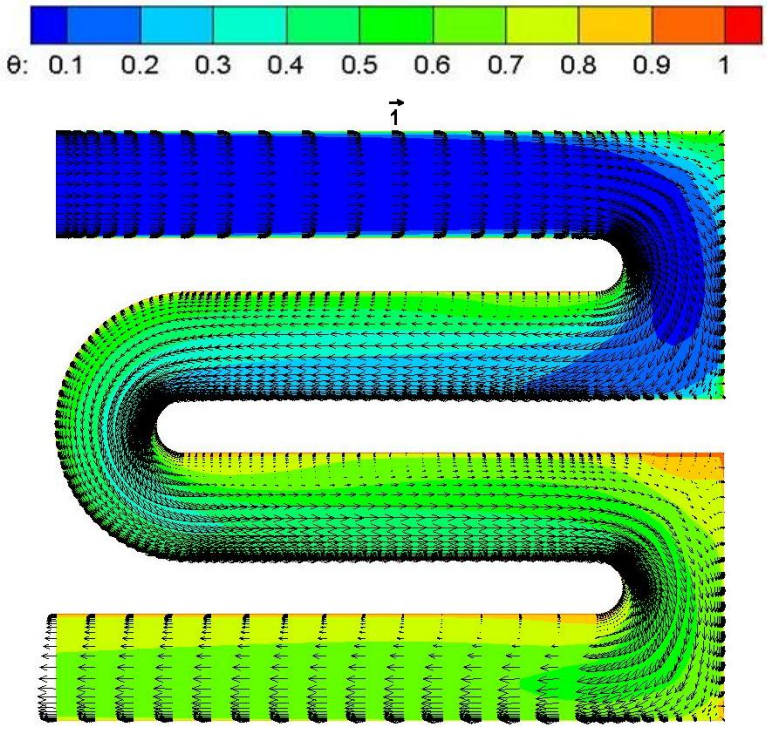

(a) Case 2: Ro=0.0, Δρ/ρ=0.115, Aspect Ratio of Whole Flowing Channel is 2:1

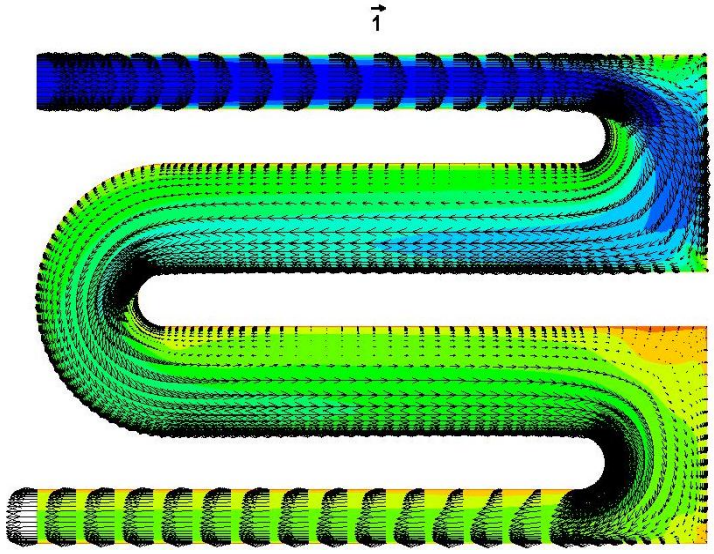

(b) Case 5: Ro=0.0, Δρ/ρ=0.115, Aspect Ratio of First and Fourth Passage is 1:1

Fig. 3.5 Velocity and temperature distribution at center portion of non-rotating four-pass channel with different inlet

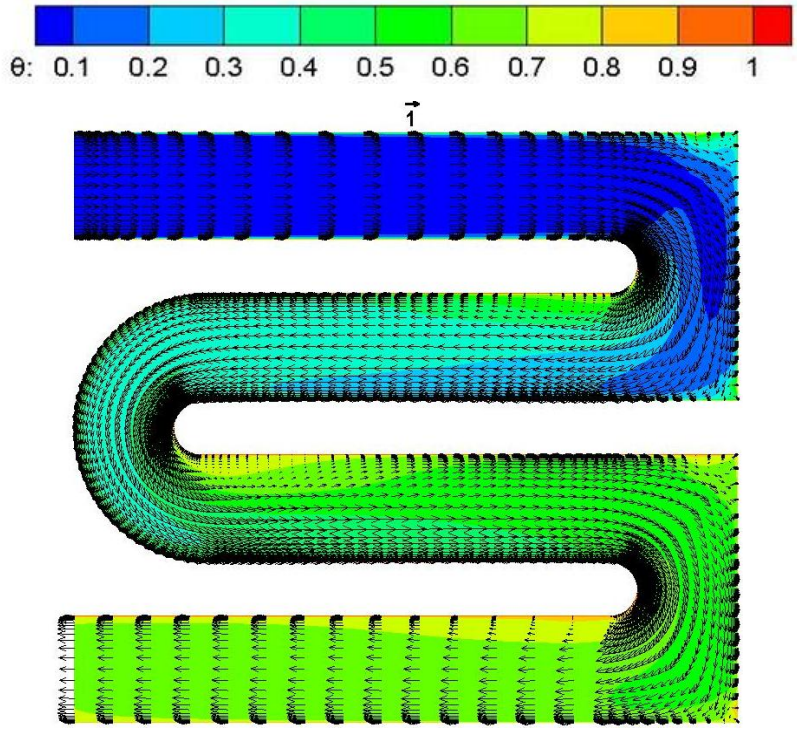

(a) Case 4: Ro=0.11, Δρ/ρ=0.115, Aspect Ratio of Whole Flowing Channel is 2:1

(b) Case 5: Ro=0.22, Δρ/ρ=0.115, Aspect Ratio of First and Fourth Passage is 1:1

Fig. 3.6 Velocity and temperature distribution at center portion of rotating four-pass channel with different inlet

Fig. 3.6 shows velocity vector and temperature distribution at the center portion of rotating flowing channels with different inlet settings. It is clear to see rotation will decrease flow attachment induced by turn effect. It also decreases the area of reverse flow. Compared to non-rotating and rotating cases, we can conclude that inlet effect only affect flow and temperature in first and second passage.

To get detailed information about inlet effect, slices at four stations will be described specially to study inlet effect to secondary flow. Fig. 3.7 shows slices used in this part to investigate effect of inlet to secondary flow and temperature distribution. Since form previous studies, inlet effect only affect flow and temperature in first two passages. The four output slices are all from these regions. Station A is the start of first sharp turn, station B is center portion of first sharp turn and station C is the exit of this turn. Station D is in the second passage, which is used to see whether inlet effect will cause influence to second half part of second passage.

Fig. 3.8 is the secondary flow and temperature distribution at stations A~D in non-rotating channel. To four-pass with same aspect ratio (AR=2) cooling channel, flow starts to attach inner surface at station A, since main flow starts to enter the first sharp turn. Secondary flow at this position is toward inner surface. At station B, it is clear to see that main cooling flow attaches inner surface area, the secondary flow here is toward outer surface and form two vortices in outer surface. At station C, since turn effect, cooling flow attaches outer surface, two vortices occur in this area. From the result at station D, it clear to see the flow attachment and secondary flow induced by first sharp turn will gradually decrease when flow moves from first sharp turn to second half part of

second passage. Compare to Case 2, flow in Case 5 shows some different behaviors, especially to flow at station B. it is clear to see instead of attachment inner surface, main flow attaches outer surface. This is because the strong inlet flow impinges outer surface at this station. This also can explain why there is a high temperature area on inner surface. The other big difference is temperature of main cooling flow in Case 5 seems be lower than Case 2. This is resulted from the diffuse of cooling flow. Unlike flow in channel with constant aspect ratio, the cross section areas of first passage and second passage of Case 5 are different. Cooling flow will diffuse, since the increase of cross section area.

Fig. 3.9 is the secondary flow and temperature distribution at stations A~D in rotating channel. Rotation effect can be seen by comparison between Case 2 and Case 3. It is revealed that since flow in first passage is radially inward flow, flow attachment occurs on trailing surface at station A. rotation also cause significant influence to flow at station B, from temperature distribution, it shows rotation moves the main cooling flow. This move also changes location and strength of vortices at this station. THE vortex which used to be on outer surface moves to inner surface and occupies most area of the cross section. The other one is closer to outer surface and become smaller than it in Case B. At station C, since flow in second passage is radially outward flow, rotation effect cause flow attachment on leading surface. With the combination of turn effect, the main cooling flow moves toward outer surface and leading surface. It changes the location and area of vortices again.

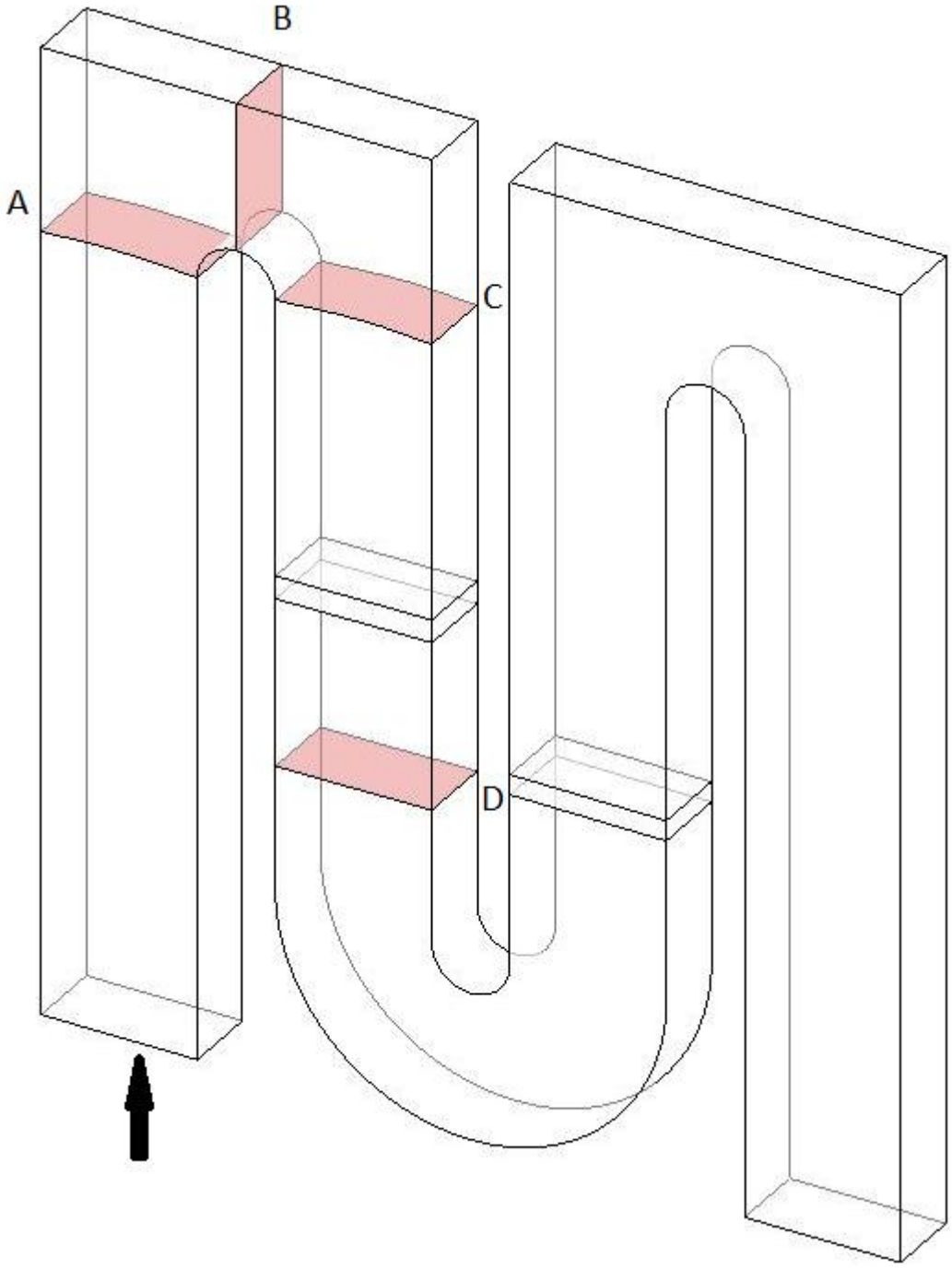

Fig. 3.7 Slices used to investigate secondary flow

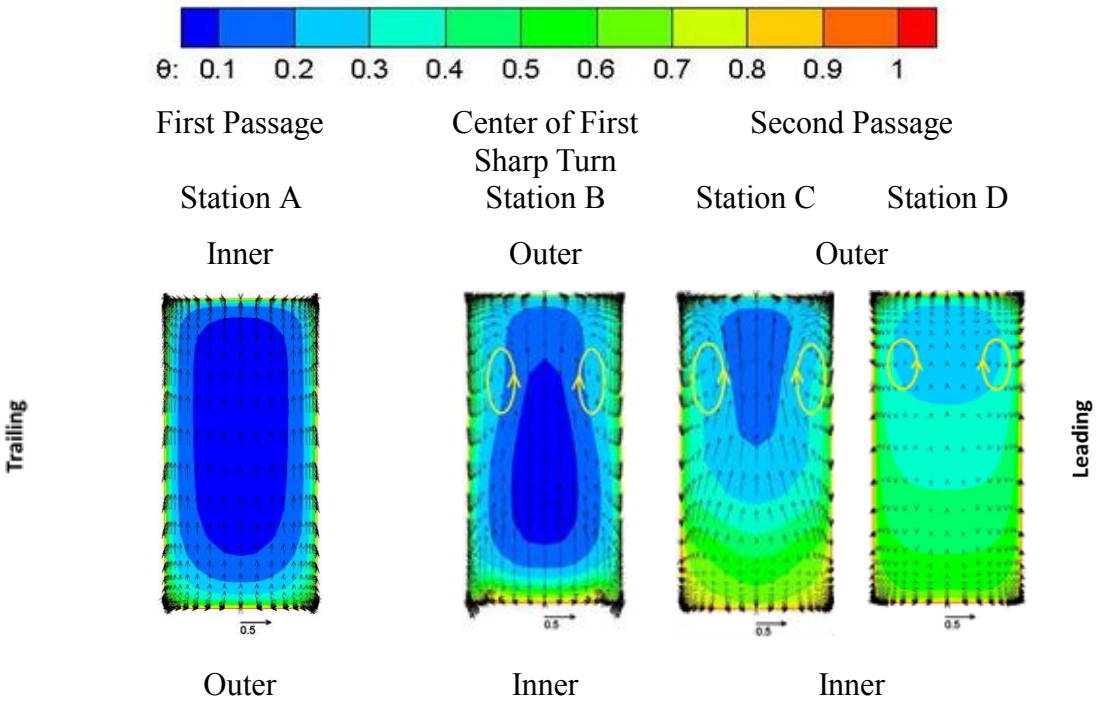

(a) Case 2: Ro=0.0, Aspect Ratio of Whole Flowing Channel is 2:1

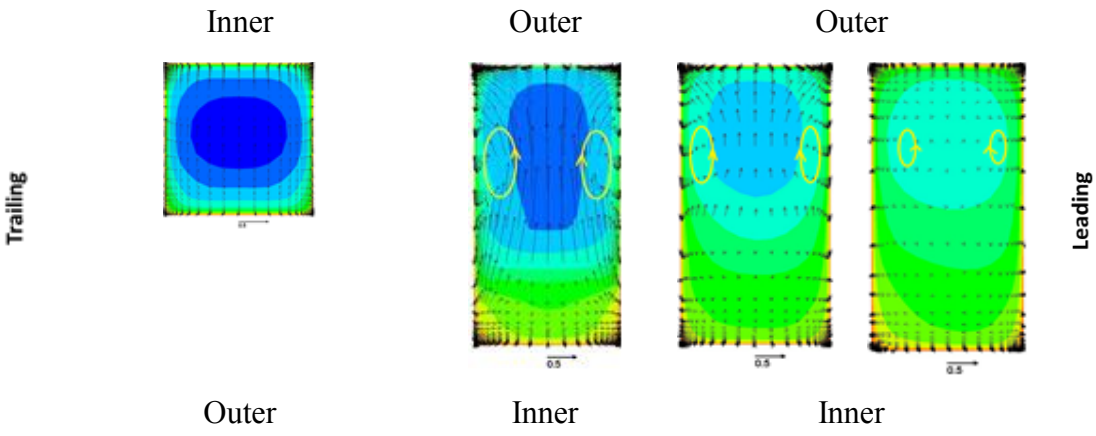

(b) Case 5: Ro=0.0, Aspect Ratio of First and Fourth Passage is 1:1

Fig. 3.8 Secondary flow and temperature distribution for non-rotating channels

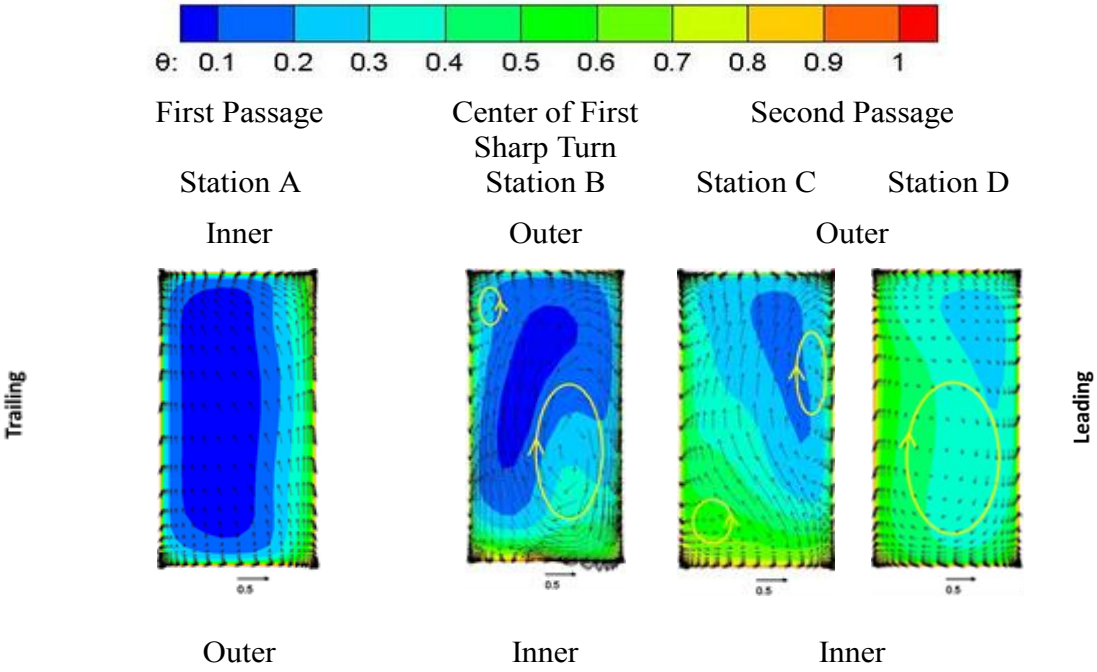

(a) Case 3: Ro=0.11, Aspect Ratio of Whole Flowing Channel is 2:1

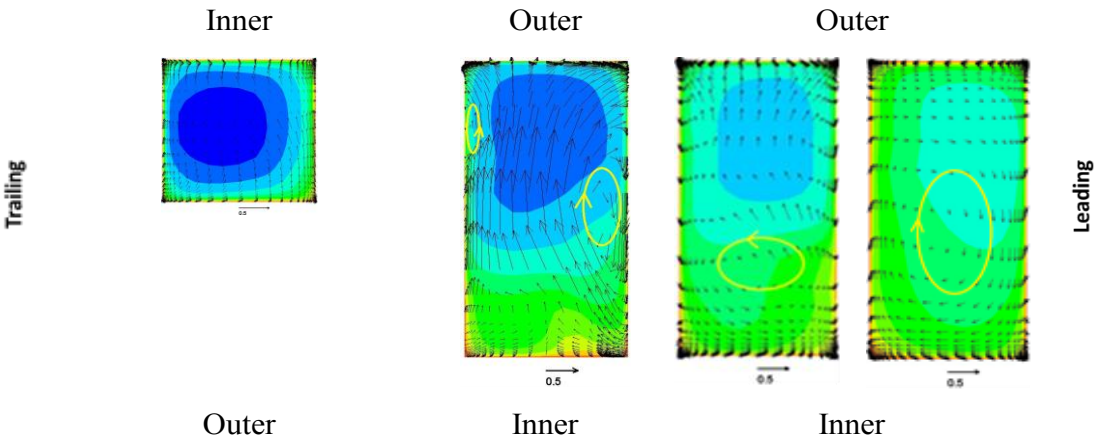

(b) Case 6: Ro=0.11, Aspect Ratio of First and Fourth Passage is 1:1

Fig. 3.9 Secondary flow and temperature distribution for rotating channels

At station D, secondary flow decreases, since it is away from first sharp turn. Main cooling flow starts to recover and cause more homogeneous temperature distribution. Compared to Case 3, result from Case 5 shows less rotation effect at station B, since stronger inlet flow here. To flow at station C and station D, rotation effect still can be seen at these two stations. However, the effect is less than it to flowing channel with identical aspect ratio (Case 2 and Case 3).

3.4.2 Heat Transfer

To discuss heat transfer enhancement, Nusselt number ratio contour and spanwise－averaged values will be used to do analysis. In Fig 3.10, according to results from Case 2, it can be seen that under non-rotating condition, high Nusselt number ratio occurs on the outer surface or first sharp turn. This is because cooling flow impinges in this portion. It also can be seen that turn effect will cause high Nusselt number ratio on one side but low values on the opposite side in after turn portions. This trend also shows in Fig. 3.11.

This big difference between Case 2 and Case 5 occurs in first passage and first sharp turn. Since the stronger cooling flow in Case 5, higher Nusselt number occurs in these portions and the values will be twice as big as Case 2. The stronger inlet flow also creates bigger reverse flow region on outer surface of second passage, which causes lower Nusselt number ratio in this region. This phenomenon can be seen in Fig. 3.10 (b) and Fig. 3.11 (b). Inlet effect also causes slight difference in smooth turn portions and

third passage. In second sharp turn and fourth passage, Nusselt number ratio of Case 5 is much higher than it in Case 2, since the change of cross-section area in fourth passage.

In these four-pass cooling channel, flows in first and third passage are radially outward flow, the Coriolis force and Buoyancy force induced by rotation will cause flow attachment on trailing surface. With higher rotation speed, this rotating effect will be more obvious. In first passage, this rotating effect should causes heat transfer enhancement on trailing surface but decrease heat transfer on leading surface. Fig. 3.12 and Fig. 3.13 clearly show this behavior. To four-pass channel with uniform aspect ratio (Case 2~4), when the rotation number equal to 0.11, Nusselt number ratio on trailing surface is increased by about 35%. However, it also causes the decrease of Nusselt number ratio on leading surface by about 25%. With the increase of rotation number from 0.0 to 0.22, the heat transfer enhancement on trailing surface is increased by about 60% and the Nusselt number ratio on trailing surface is decreased by about 30%. In second and fourth passage, the rotating effect cause positive influence on heat transfer on leading surface but negative influence on trailing surface.

Fig. 3.14 is Nusselt number ratio for rotating channels. In four-pass with square inlet (AR=1:1 in first passage), when rotation number equal to 0.11, Nusselt number ratio on leading surface will be decreased by about 10%, However, on trailing surface, Nusselt number ratio will be increase by about 15%. When rotation number equal to 0.22, compared to non-rotating case (Case 5), Nusselt number ratio on leading surface will be decreased by about 20% but be increased on tailing by about 25%. Compared to Case 2~4, these fluctuations are smaller.

Nu/Nu_0

Leading

Trailing

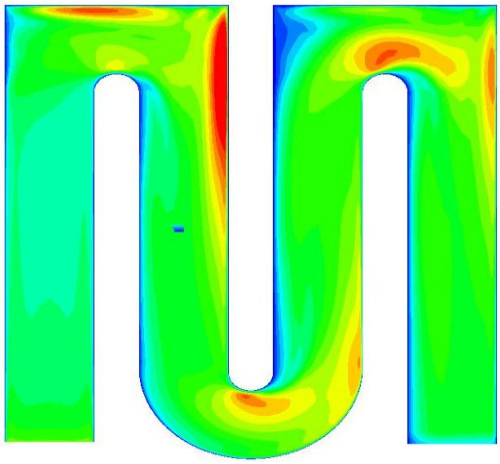

(1a) Case 2: Ro=0.0, Aspect Ratio of Whole Flowing Channel is 2:1

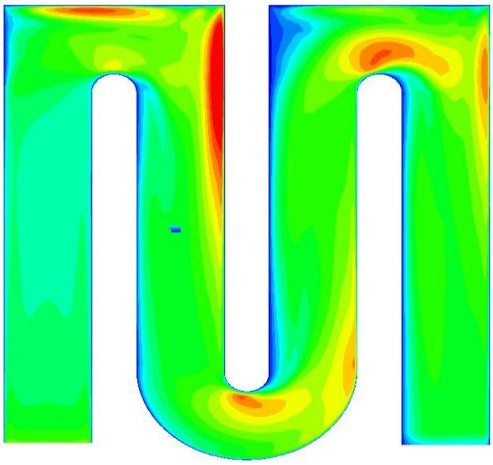

(1b) Case 2: Ro=0.0, Aspect Ratio of Whole Flowing Channel is 2:1

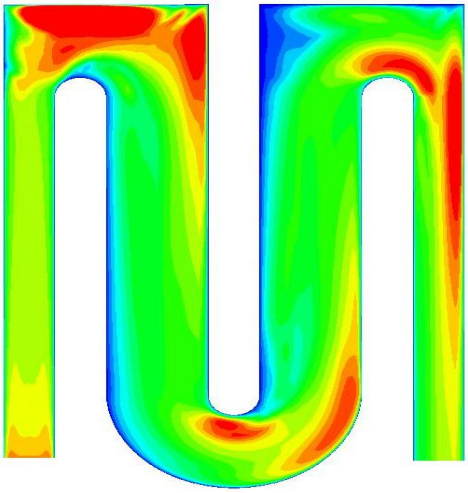

(2a) Case 5: Ro=0.0, Aspect Ratio of First and Fourth Passage is 1:1

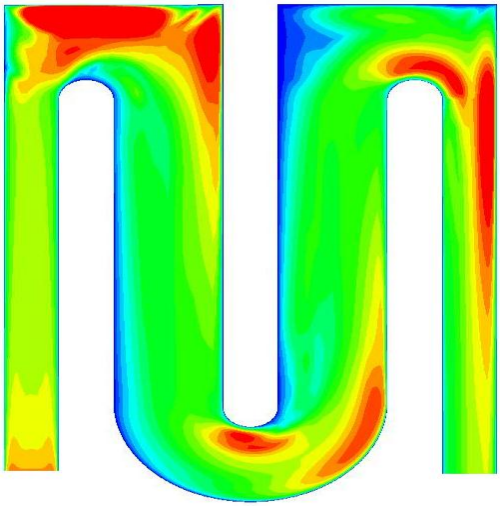

(2b) Case 5: Ro=0.0, Aspect Ratio of First and Fourth Passage is 1:1

Fig. 3.10 Nusselt number ratio contour on (a) leading surface and (b) trailing surface of non-rotating channels with different inlet

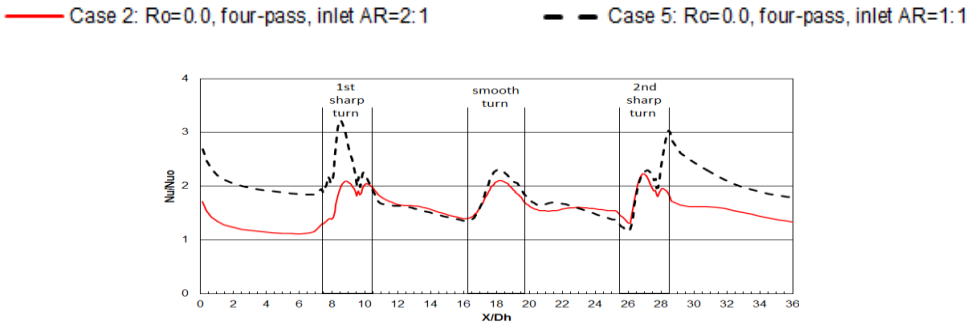

(a) Leading surface

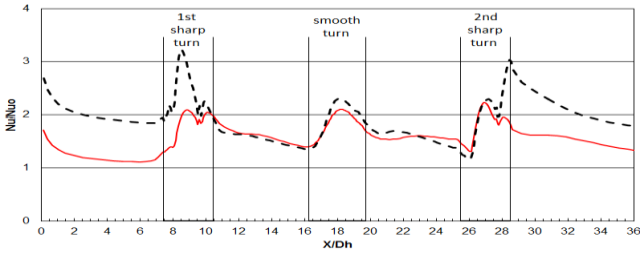

(b) Trailing surface

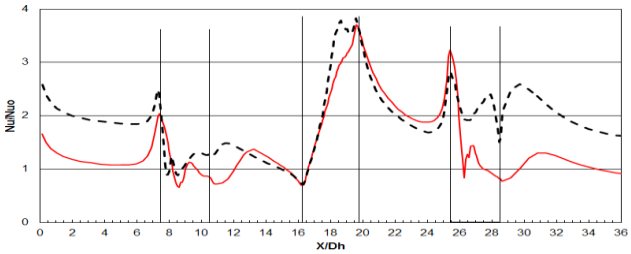

(c) Inner surface

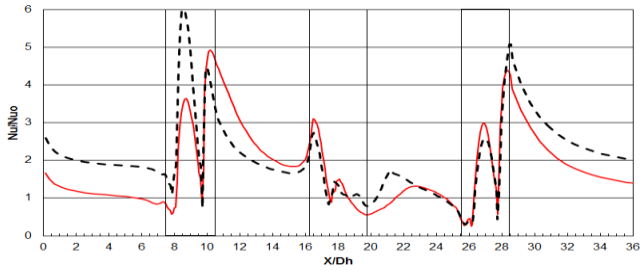

(d) outer surface

Fig. 3.11 Spanwise-averaged Nusselt number ratio for non-rotating

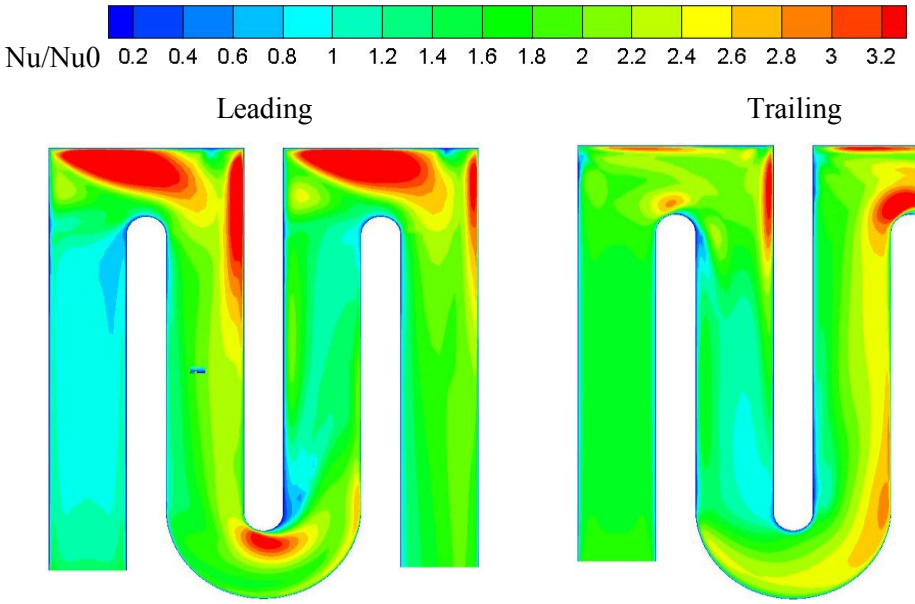

(1a) Case 3: Ro=0.11, Aspect ratio of Whole Flowing Channel is 2:1

(1b) Case 3: Ro=0.11, Aspect Ratio of Whole Flowing Channel is 2:1

(2a) Case 6: Ro=0.11, Aspect Ratio of First and Fourth Passage is 1:1

(2b) Case 6: Ro=0.11, Aspect Ratio of First and Fourth Passage is 1:1

Fig. 3.12 Nusselt number ratio contour on (a) leading surface and (b) trailing surface of rotating channels with different inlet (Ro=0.11)

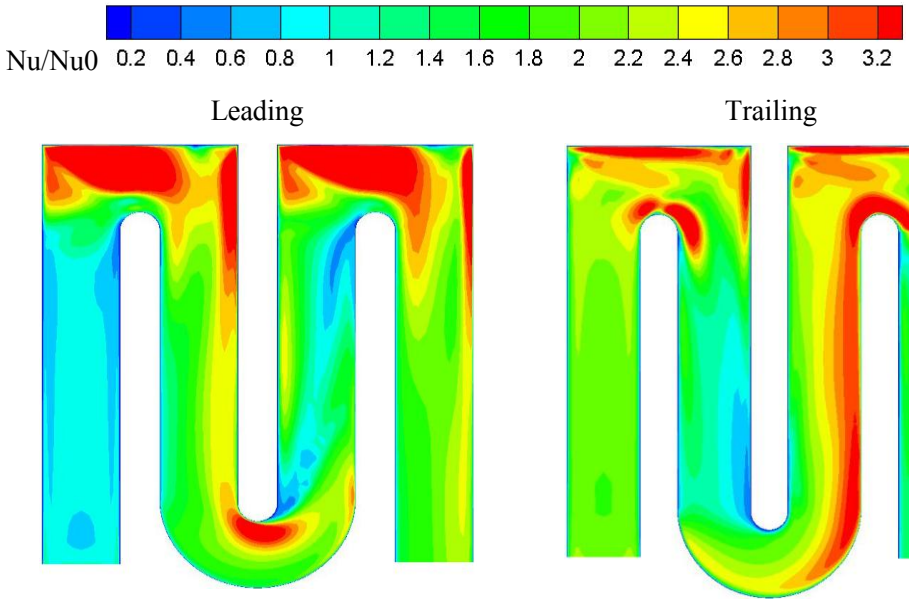

(1a) Case 4: Ro=0.22, Aspect Ratio of Whole Flowing Channel is 2:1

(1b) Case 4: Ro=0.22, Aspect Ratio of Whole Flowing Channel is 2:1

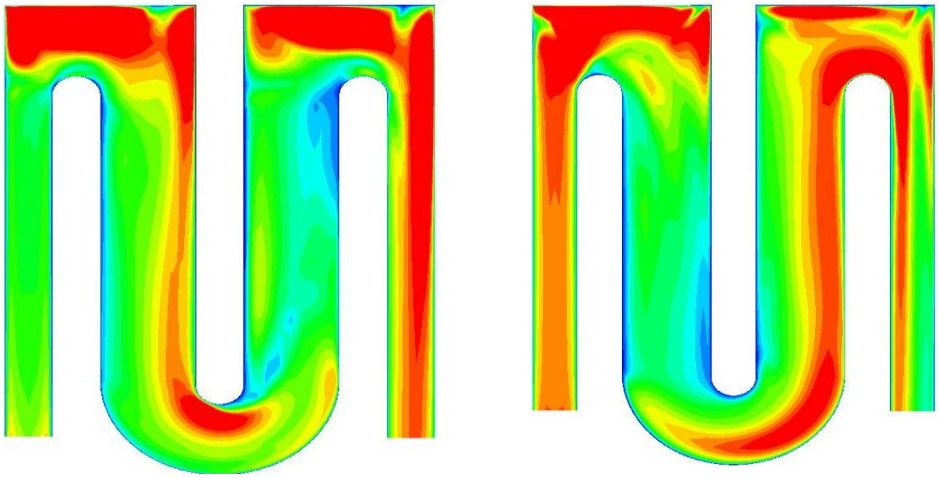

(2a) Case 7: Ro=0.22, Aspect Ratio of First and Fourth Passage is 1:1

(2b) Case 7: Ro=0.22, Aspect Ratio of First and Fourth Passage is 1:1

Fig. 3.13 Nusselt number ratio contour on (a) leading surface and (b) trailing surface of rotating channels with different inlet (Ro=0.22)

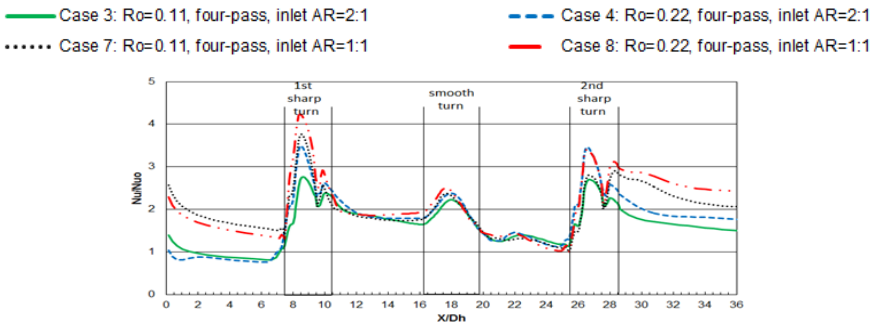

(a) Leading surface

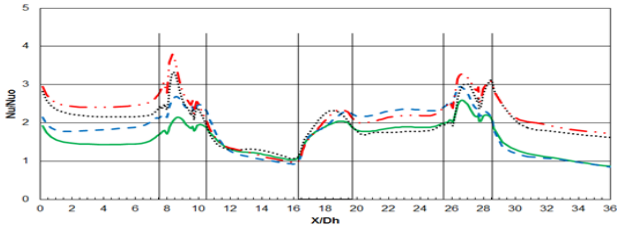

(b) Trailing surface

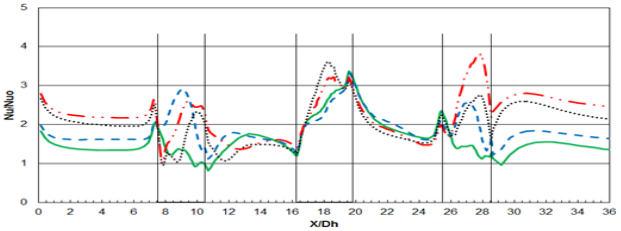

(c) Inner surface

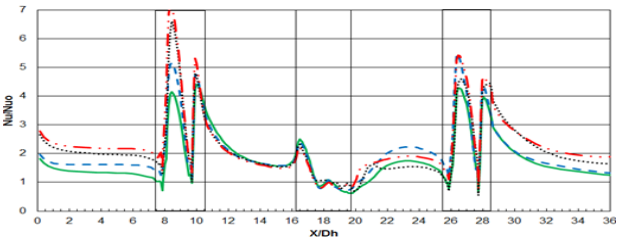

(d) outer surface

Fig. 3.14 Spanwise-averaged Nusselt number ratio for rotating channels

CHAPTER IV

FLOW AND HEAT TRANSFER IN A MULTI-PASS CHANNEL WITH AND WITHOUT VANE

In this chapter, results gained from second moment closure model will be represented to analyze vane effects in a four-pass channel. Numerical results will also be compared to experiment data in Lei et al. [15].

4.1 Description of Geometry

The geometry of the internal cooling channel used in the experiment of Lei et al. [15] is shown in Fig 4.1. Four straight ducts and three turn portions are used to combine this four-pass channel. The first passage and the forth passage are square (AR=1:1) ducts, the second passage and the third passage are rectangular (AR=2:1) ducts. First duct and second duct are connected by a sharp turn. Similar arrangement is used to connect third passage and fourth passage. As to second passage and third passage, they are connected by a turn with round corner. Vane will be added in this smooth turn portion.

The objective of the experiment in Lei et al. [15] is to investigate vane effect; they only heat second and third passages. In order to do comparison with experiment, we will also mainly focus on the flow and heat transfer in second passage (part before smooth turn), smooth turn portion and third passage (part after smooth turn). Hydraulic diameter will be calculated based on the dimension of the rectangular passages. The

Hydraulic diameter, D_h, in this geometry is 0.67in (16.9mm). The distance from the rotating axis to the center of the flowing channel, $Rr/D_{h,}$ is equal to 39. The maximum length of the channel, L/Dh, is about 9.4.

4.2 Description of Computational Grid

Computational geometry used in this research is shown on Fig 4.2. Refer to the experiment configuration (Fig. 4.1); cooling air flows from circular pipe into main flowing channel, the circular pipes are partially connected to main flowing channel. In order to closely simulate real flowing situation, circular pipes are added to be inlet and outlet with length equal to 64 mm. The rotation angle, β, is the angle between rotation axis and direction of rotation. In this figure, the direction of rotation is +z axis and rotation axis is -y axis. Thus, rotation angle, β=90°.

Fig. 4.3 is the grid independent test for four-pass channel used in this part. This is focus on the grid number used in main flowing channel. Two grid sets are used to do grid independent test: (1) Grid 1, 61×41 grid numbers on cross section and 401 grid numbers on streamwise direction. (2) Grid 2, 41×33 on cross section and 501 on streamwise direction. According to these results, in this research, the grid points used in cross section of main flowing channel are 61×41. As to stream-wise direction, 401 grid points are used. With the combination of grid numbers in circular inlet and outlet, grid number used in the channel without addition of vane is 1.3 million grid points. As to smooth with vane cases, two million additional grid points will be used in turn portion. Total grid number in these cases is 1.5 million grid points.

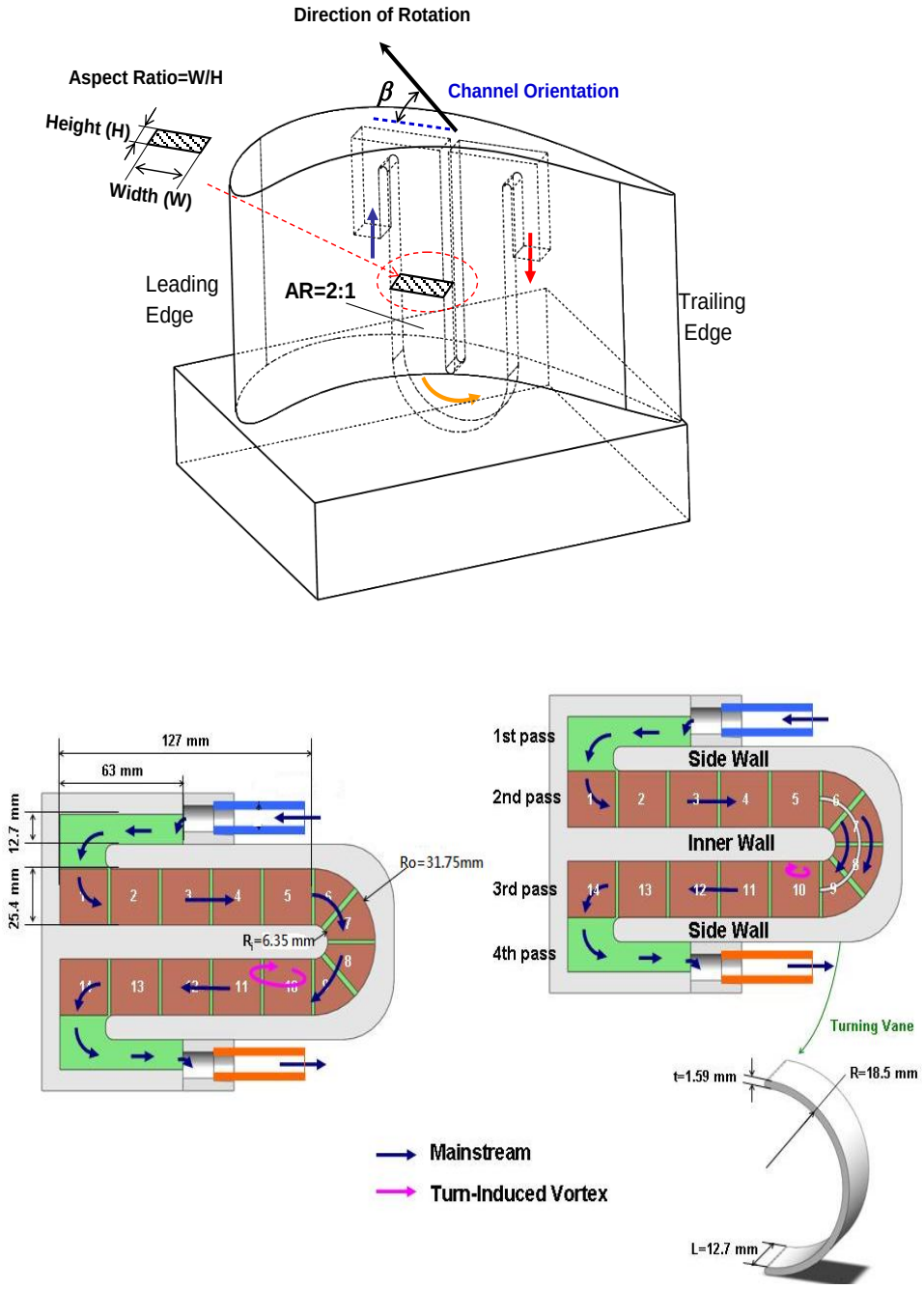

Fig. 4.1 Geometry of four-pass channel used in experiment (from Lei et al. [15])

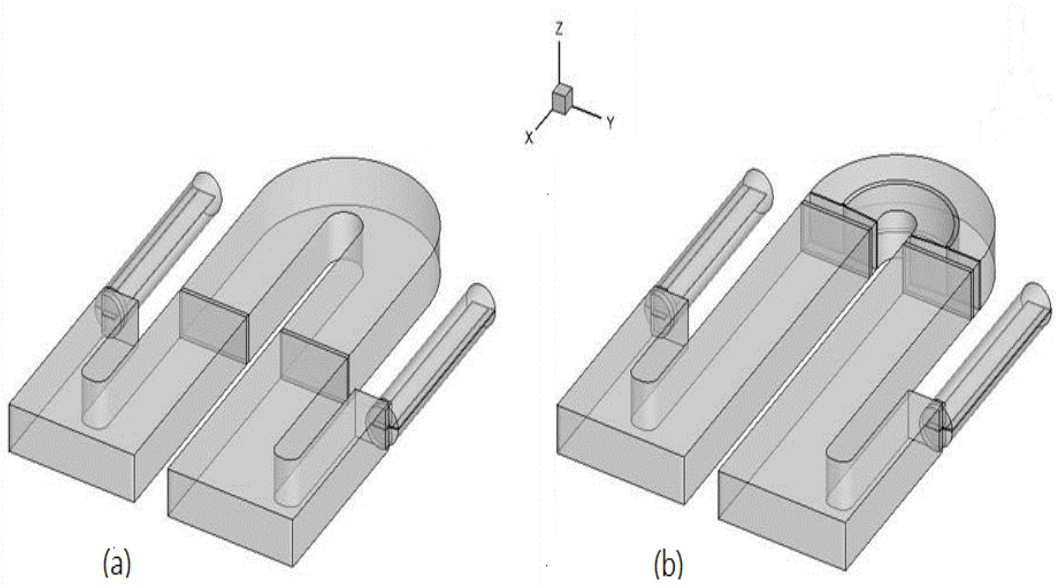

Fig. 4.2 Computational geometry used in (a) without vane cases (b) with vane cases

Case No.	Re	$\Delta\rho/\rho$	Ro	β	With or Without Vane
1	20,000	0.12	0.0	-	Without Vane
2	20,000	0.12	0.0	-	With Vane
3	20,000	0.12	0.2	90	Without Vane
4	20,000	0.12	0.2	90	With Vane
5	20,000	0.12	0.4	90	Without Vane
6	20,000	0.12	0.4	90	With Vane
7	20,000	0.22	0.2	90	Without Vane
8	20,000	0.22	0.2	90	With Vane
9	20,000	0.32	0.2	90	Without Vane
10	20,000	0.32	0.2	90	With Vane
11	20,000	0.22	0.2	45	Without Vane
12	20,000	0.22	0.2	45	With Vane

Table 4.1 Summary of cases studied for vane effect

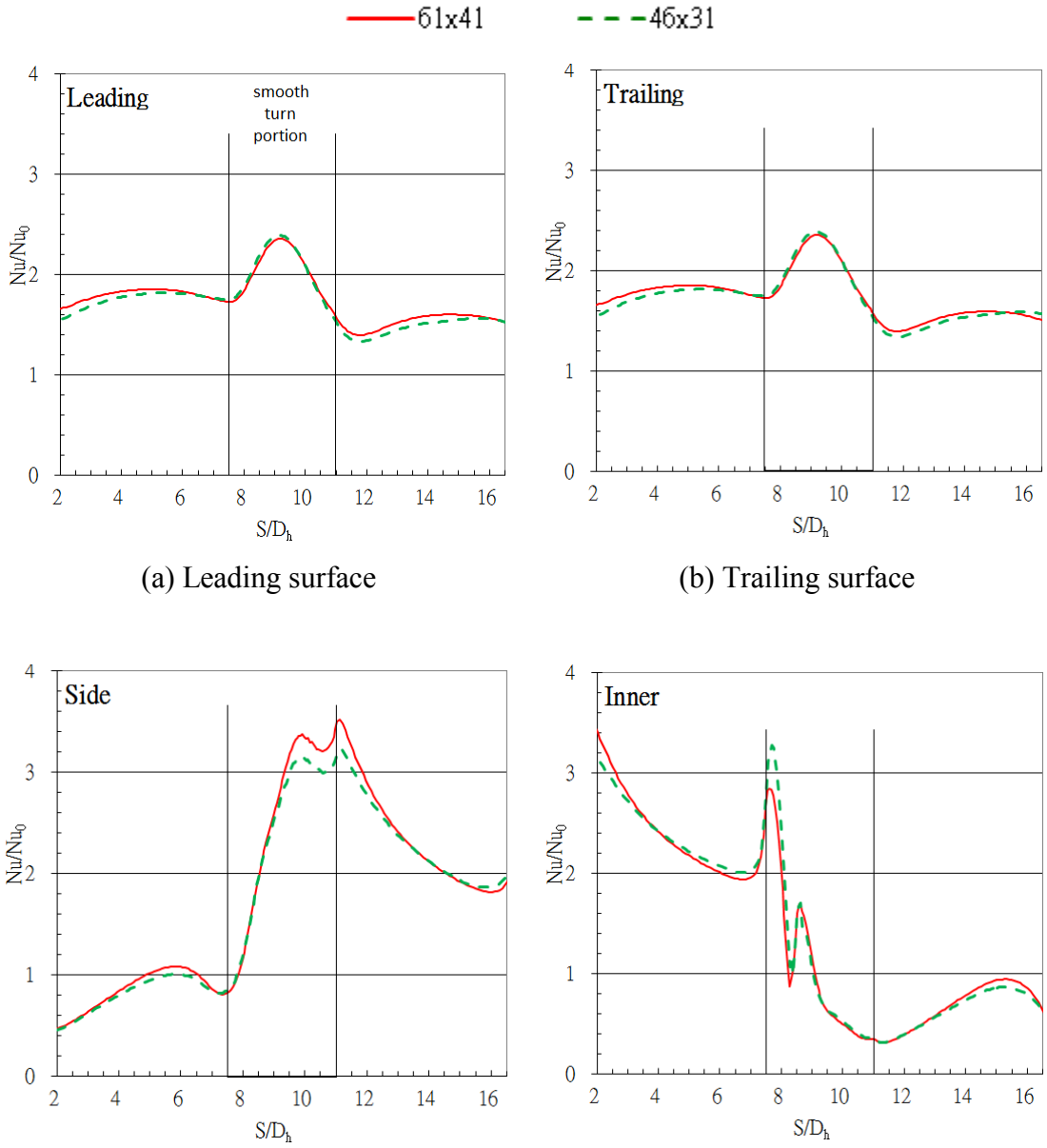

(a) Leading surface

(b) Trailing surface

(c) Side surface

(d) Inner surface

Fig. 4.3 Grid independent test

4.3 Case Study

Table 4.1 shows the summary of cases studied in this chapter**.** There are four cases used to evaluate vane effect under non-rotating condition and rotating condition, with Reynolds number, Re, equals to 20k and inlet density ratio, $\Delta\rho/\rho$, equals to 0.12.

Different rotation number (Ro) will be set from 0.0~ 0.2 to investigate rotating effects.

4.4 Velocity and Temperature Field

Since the objective of this research is to study vane effect, some parts will be output to get detailed information about vane effect. Fig. 4.4 shows geometry needed for this request, it includes second passage (part before smooth turn), smooth turn portion and third passage (part after smooth turn). This U-shaped duct will be showed specially.

Fig. 4.5 shows velocity vector and temperature distribution at the center portion of this U-shaped duct. According to results from Case 1, when the flowing channel is under non-rotating condition, in part before smooth turn, main cooling stream will attaches on inner surface and reverse flow region occurs on the side surface. This is because the turn effect resulted from first sharp turn. Similar effect happens in the part after smooth turn. Temperature distribution also reflects this phenomenon. In the part before smooth turn, temperature on inner surface is cooler than it on side surface, since main cooling flow attaches on inner surface.

Compared to results from Case 1 and Case 2, it is easy to see that the addition of vane will not cause significant influence to part before it. However, in smooth turn

portion, the addition of vane divides flowing channel into two sub-channels. Main cooling flow is also divided into two minor flows. From velocity vector, it is easy to see that more cooling stream flows into inner sub-channel. Temperature distribution also shows that temperature in inner sub-channel is cooler than it in outer sub-channel.

This vane effect lasts to part after smooth turn. With the addition of vane, flow attachment on the side surface vanishes. From Fig. 4.5 (b), it shows that main cooling stream flows in the center portion of this part.

Fig. 4.5 (c) shows result from Case 3, when the cooling channel is under rotating condition; main cooling stream is more uniformly flows into second passage. This is because rotation will make flow mixing. This is so-called rotation effect, it decrease flow attachment and reverse flow induced by turn effect. From temperature distribution, rotation effect causes temperature of flow in the turn portion and part after turn become more homogeneous. Compared to result from Case 2, result from Case 4 shows that with the mixing induced by rotation, the difference between flow in inner sub-channel and flow in out-sub-channel becomes smaller, no matter in velocity vector or temperature distribution.

It is well known that secondary flow plays an important role in velocity field and local heat transfer. Turn effect can cause it happen, since it changes flowing direction of main stream. Rotation can change it too. Because it induces Coriolis force. Temperature difference induces Buoyancy force, which also can cause significant influence to secondary flow. To get more detailed understanding related to secondary flow, different slices will be shown in the later part.

Fig. 4.4 shows slices which will be described to study secondary flow specially. There are five stations in this figure, station A is at the position after first sharp turn, station B is at the start of the smooth turn, station C is the center portion of smooth turn, where degree equals to 90°, Station D is at the end of the smooth turn, slice E is the near the end of third passage.

Fig 4.6 is temperature distribution of U-shaped duct. Compared to non-rotating cases, it is easy to see that rotation effects changes main cooling stream, which causes different Nusselt number ratio.

Fig 4.7 is the secondary flow and temperature distribution at each station of non-rotating channel. Result form Case 1 shows strong flow attachment on inner surface, which is resulted from first sharp turn. Two vortices with opposite rotating direction occur in this region. When flow moves from station A to station B, turn effect decreases due to the distance. In the smooth turn portion, secondary flow at station C is toward side surface and two vortices occur in this region. The main cooling stream is close to the inner wall region. After smooth turn portion, turn effect induced by smooth turn causes flow attachment on the side surface, it is easy to see cooling air is close to side surface at station D. Two vortices with opposite rotating direction are generated by the secondary flow in side wall region. It is also revealed that this turn effect decreases when flow moves from station D to Station E.

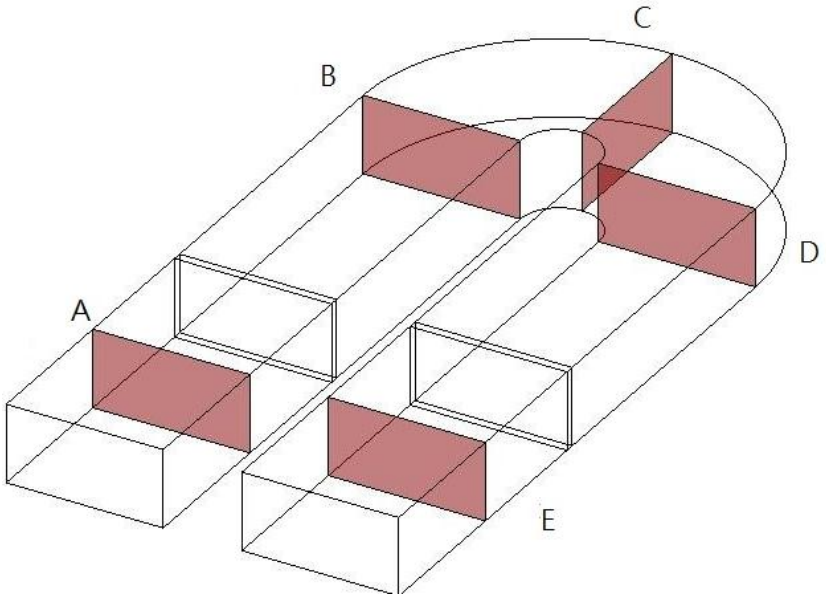

(a)

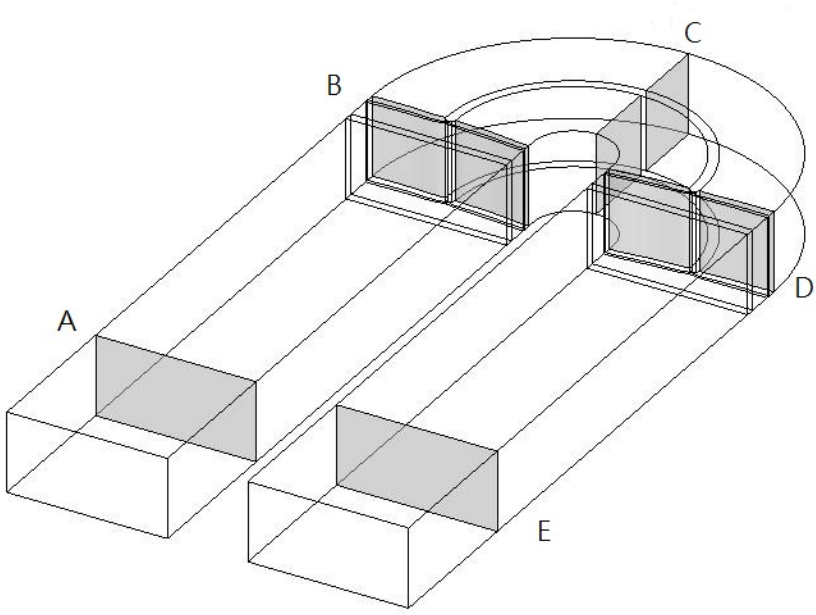

(b)

Fig. 4.4 Geometry of second passage, smooth turn portion and third passage. (a) without addition of vane. (b) with addition of vane

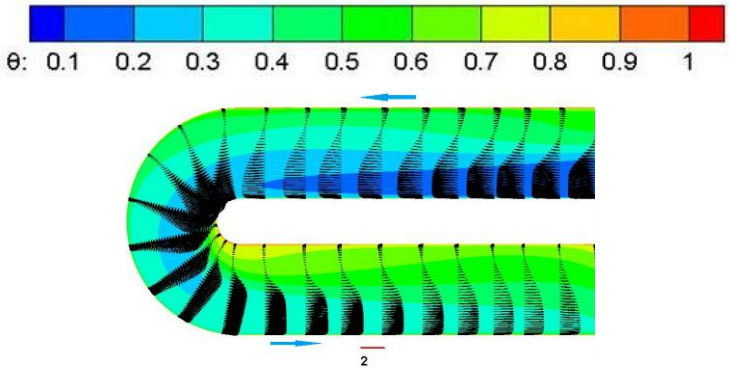

(a) Case 1: Ro=0.0, Δρ/ρ=0.12, Without Vane

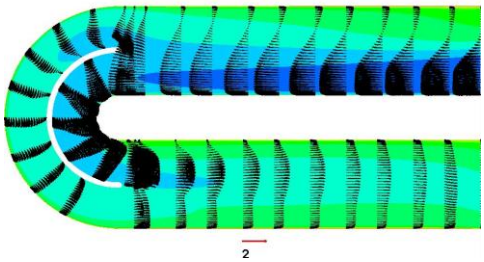

(b) Case 2: Ro=0.0, Δρ/ρ=0.12, With Vane

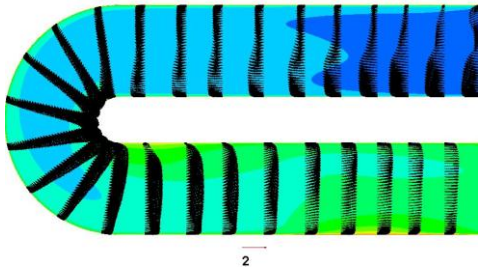

(c) Case 3: Ro=0.2, Δρ/ρ=0.12, β=90, Without Vane

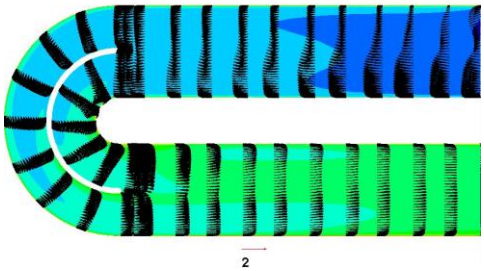

(d) Case 4: Ro=0.2, Δρ/ρ=0.12, β=90, With Vane

Fig. 4.5 Velocity and temperature distribution at center portion of U-shaped duct

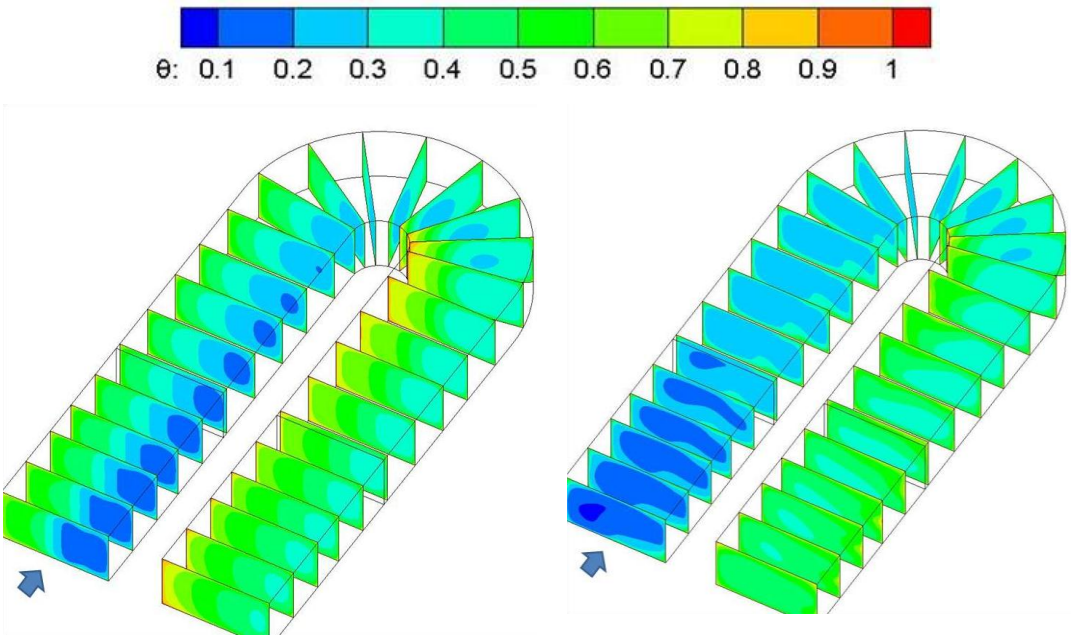

(a) Case 1: Ro=0.0, Δρ/ρ=0.12, Without Vane

(b) Case 2: Ro=0.0, Δρ/ρ=0.12, With Vane

(c) Case 3: Ro=0.2, Δρ/ρ=0.12, β=90, Without Vane

(d) Case 4: Ro=0.2, Δρ/ρ=0.12, β=90, With Vane

Fig. 4.6 Temperature distribution of U-shaped duct

Compared to result gained from Case 1, result from Case 2 shows identical secondary from and temperature distribution at station A. It shows that the addition of vane in smooth turn portion does not cause significant variation in part before smooth turn. At station B, the addition of vane divides main cooling stream into two minor streams, most cooling streams flows into inner sub-channel. However, the strong secondary flow shows in outer sub-channel. In the smooth turn portion, there are four vortices occurs at station C, two for each sub-channels. Although the numbers of vortices are the same, the vortices in inner sub-channel show stronger strength. This is because the stronger secondary flow in inner sub-channel. At station C, it also revealed that flow attachment occurs in near vane region of inner sub-channel. This situation lasts to station D and Station E, which is the main reason to why temperature distribution in Case 2 is different to it in Case 1 at these stations.

Secondary flow and temperature distribution at each station of rotating channel are shown in Fig. 4.8. Results form Case 3 clearly shows that rotating effect decreases the flow attachment induced by first sharp turn and causes cooling stream attaches leading surface of second passage (station A and B). At station A, three vortices occur, which are induced by the rotating effect. At station B and C, only one big vortex occupies almost whole area and rotates in counter-clockwise direction. In third passage (after smooth turn), since the flow moves from hub to tip, the rotation causes cooling air attaches trailing surface.

Compared to results from Case 2, results from Case 4 shows flow attachment at station A due to rotation effect. At station B, two vortices with same rotating direction

occur, one for each channel. At station C, Flow attachment in near vane area of inner sub-channel still can be seen in Case 4. However, the strength is lower than it in Case 2. In Case 2, after two minor streams combination, main cooling stream flows in center portion at station E. However, in Case 4, nearly homogeneous temperature distribution is shown on slice at station E.

Compared to results in Case 3 and Case 4, it can be seen that the addition of vane in smooth turn portion cut the main cooling stream into two minor streams. It also cut the big vortex at station B, C, D into two vortices with same rotating direction. Similar effect also can be seen in temperature distribution.

4.5 Pressure Loss

The original objective to add a vane in turn portion is to reduce the pressure loss occurs in this portion. Fig. 4.9 is the spanwise-averaged pressure of non-rotating cooling channel with /without vane. It is clear to see that with the addition of vane, pressure loss can be decreased.

According to table 4.2, with the addition of vane, pressure loss can be reduced by about 55%.

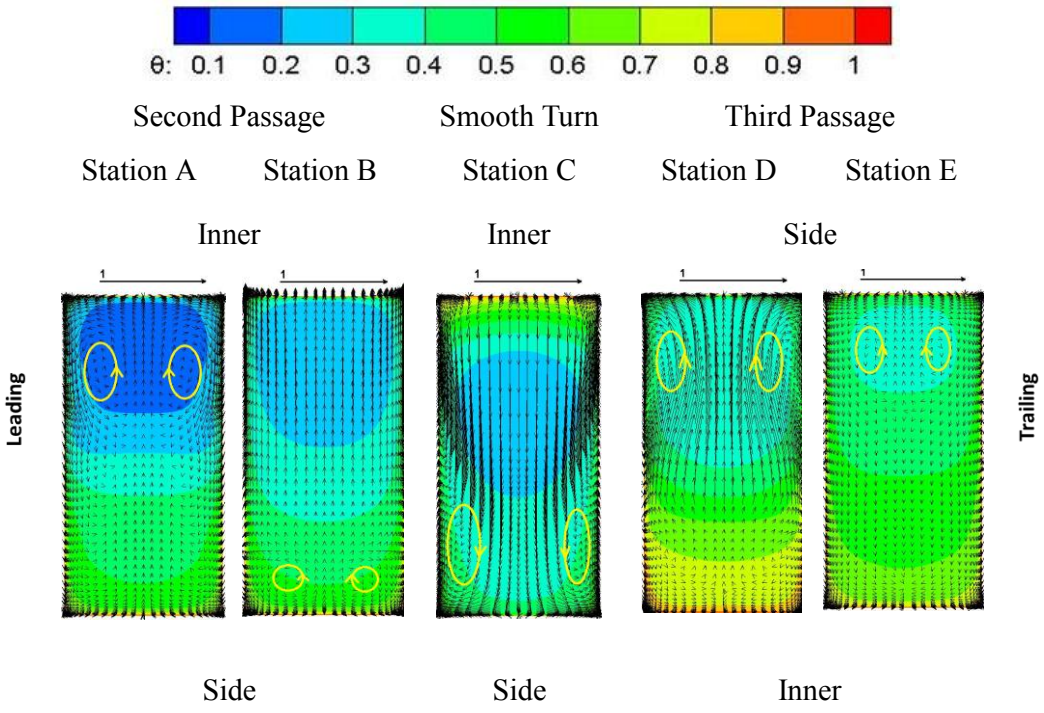

(a) Case 1: Ro=0.0, $\Delta\rho/\rho$ =0.12, Without vane

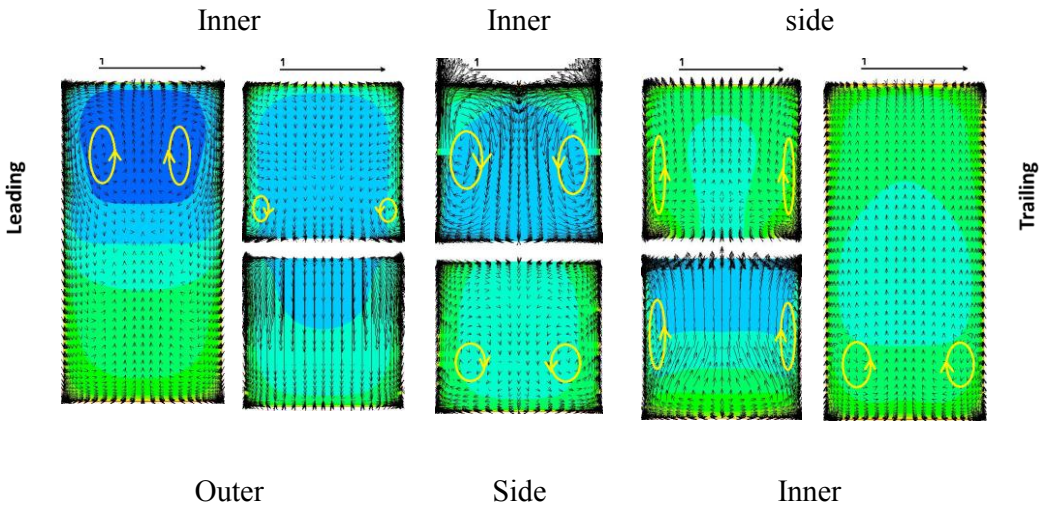

(b) Case 2: Ro=0.0, $\Delta\rho/\rho$ =0.12, With vane

Fig. 4.7 Secondary flow and temperature distribution for non-rotating channels

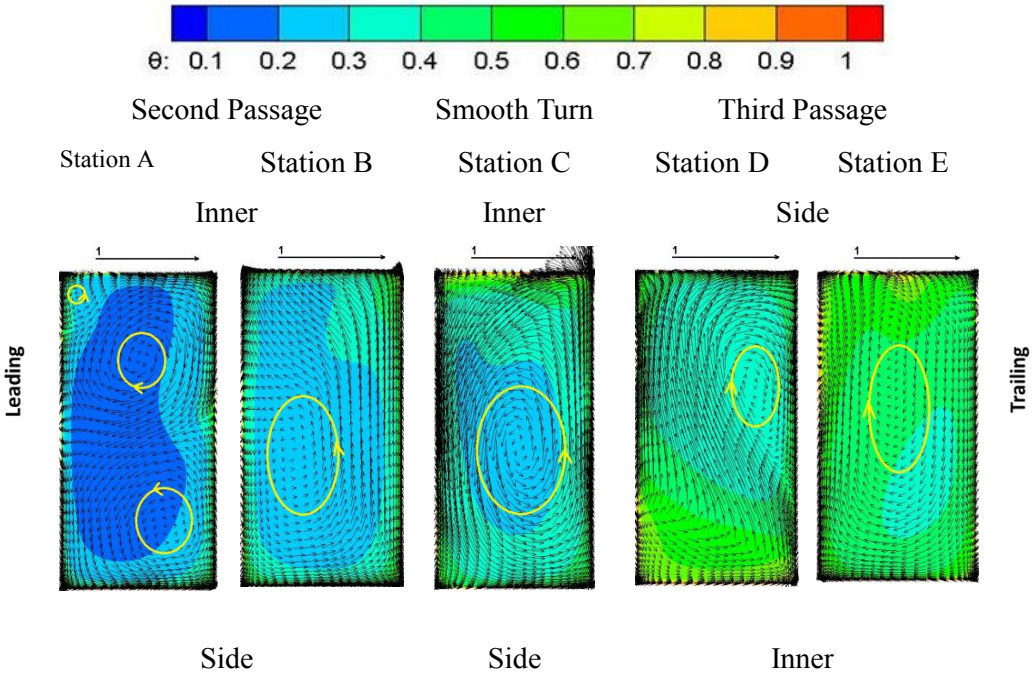

(a) Case 3: Ro=0.2, $\Delta\rho/\rho$=0.12, β=90°, Without Vane

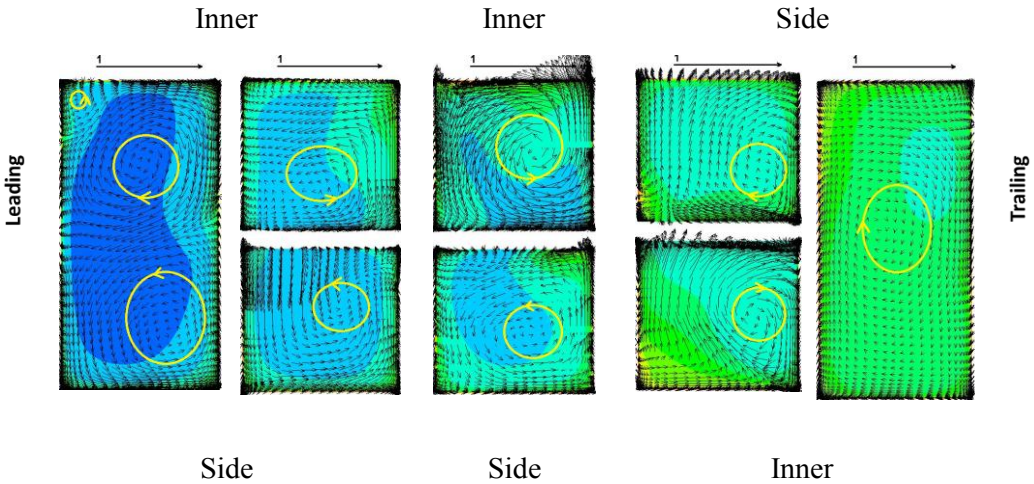

(b) Case 4: Ro=0.2, $\Delta\rho/\rho$=0.12, β=90°, With Vane

Fig. 4.8 Secondary flow and temperature distribution for rotating channels

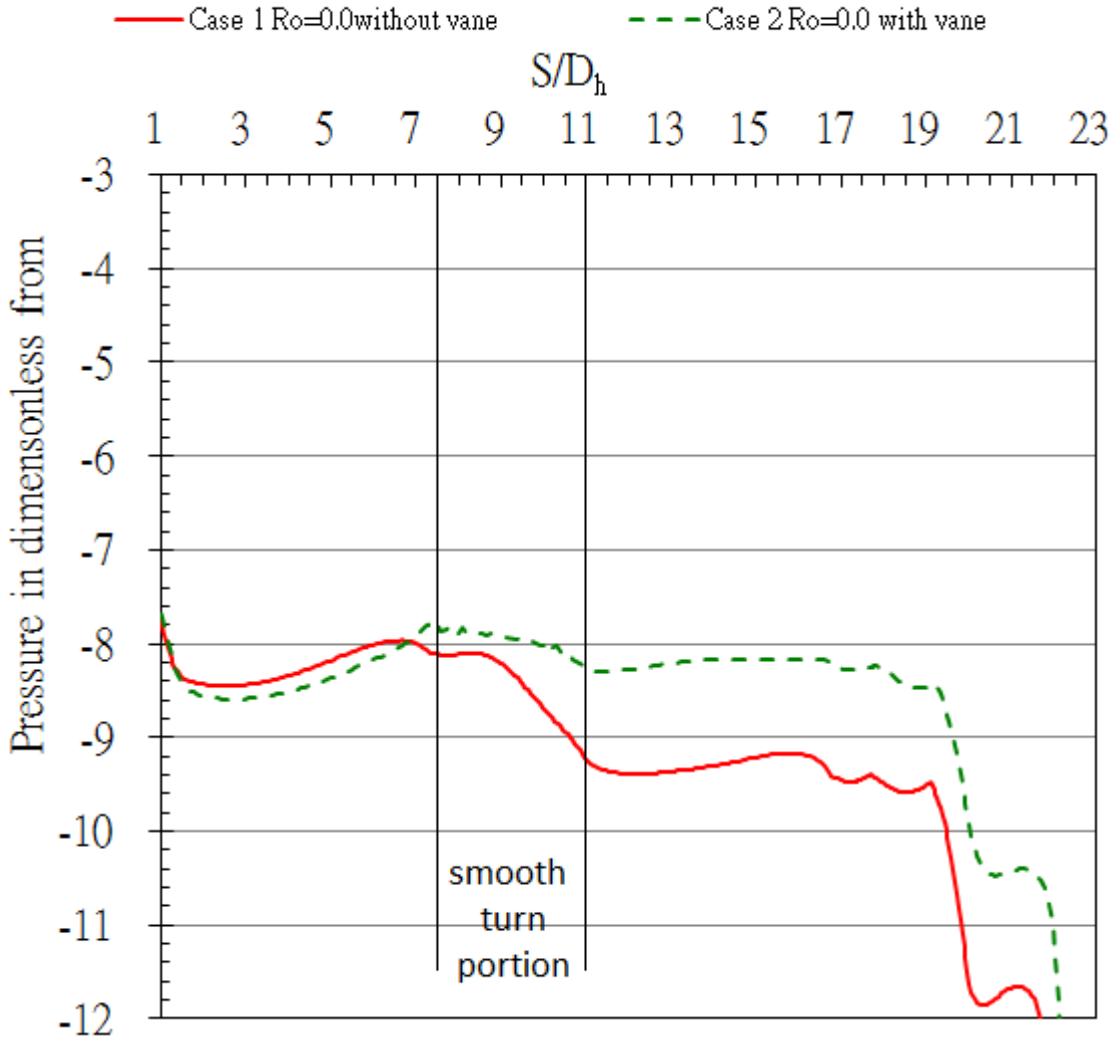

Fig. 4.9 Effect of vane on pressure loss for non-rotating channel

	Case 1: Ro=0.0, without vane	Case 2: Ro=0.0, with vane
Pressure loss	1.1	0.5

Table 4.2 Pressure loss for non-rotating channels with /without vane

4.6 Heat Transfer

In this part, Nu/Nu_0 ratio will be used to see heat transfer enhancement. Nu_0 is Dittus-Boelter correlation, which was mentioned in chapter 3.

Fig. 4.10 is Nusselt number ratio on leading and surface gained from Case 1~4. Results from case 1 show high Nusselt number ratio occurs on the inner surface of second passage (part before smooth turn), which is because strong flow attachment this region. On the side surface of this part, the Nusselt number ratio is very low; this also can be seen in spanwise-averaged Nusselt number ratio in Fig. 4.11. The reason to cause this is the strong reverse flow in this area. In the smooth turn portion, high Nusselt number ratio occurs in inner wall region, which is related to the flow attachment in this region. To part after smooth turn, Nusselt number ratio in near side surface region is higher than it in near inner surface region due to the flow attachment induced by smooth turn. Nusselt number ratio distribution on leading and trailing surface of Case 1 is almost identical.

Compare to case 1, Nusselt number ratio contour of case 2 shows similar distribution in the region before smooth turn. The big difference between these two cases is in smooth turn portion. In this portion, most cooling stream flows into inner sub-channel, which causes high Nusselt number ratio in the inner surface region. Nusselt number ratio in outer sub-channel is much lower than it in inner sub-channel. According to Fig. 4.7(b), it is clear to see that secondary flow in inner sub-channel pushes the cooling stream to near vane region. This causes high Nusselt number ratio in this region and can be seen in Fig. 4.10. Since more cooling stream flows into inner sub-channel, it

also changed Nusselt number distribution in part after smooth turn. Compared to Case 1, the addition of vane increase Nusselt number ratio on inner surface but decrease it on side surface.

When the channel is under rotating, flow attachment induced by first sharp turn decreased. On the leading surface, rotating effect cause strong heat transfer. Under this condition, with the strong secondary flow induced by rotation, low heat transfer area in near side surface region gets improved. In the smooth turn portion, heat transfer on the inner surface is still high, but the value is not as high as it in case 1. The secondary flow in this region causes temperature mixing, which cause temperature gradient decrease. This is the reason Nusselt number ratio distribution in this area is more homogeneous than it in case 1. After smooth turn, rotation cause opposite effect, it lowers heat transfer on leading surface but increase heat transfer on trailing surface.

In Case 2, it shows that Nusselt number ratio in inner sub-channel is much higher than it in outer-sub-channel. According to result from Case 4, it shows rotation can decrease the difference between these two cases. Since cooling stream almost equally flows into two sub-channels. Besides, the Nusselt number ratio of near vane region of inner sub-channel is still high but the value is not as high as it in case 2.

Fig. 4.11 is spanwise-averged Nusselt number ratio for non-rotating channel with and without vane (Case 1 and 2). Experiment data in Lei et al. [15] will be added in this part to do comparison. On leading and trailing surface, numerical results on these two surfaces are identical. To parts before smooth turn, both experiment data and numerical result shows the addition of vane does not cause significant influence to

Nusselt number ratio in this region. This is consistent with previous conclusion. In the smooth turn portion, experiment data shows that the addition of vane only reduces the values; it does not change the trend. And the peak value occurs at position near the exit of turn. However, in numerical results, the addition of vane flats the fluctuation in this portion, the distribution looks like a horizontal line. Compared to values in experiment data, second moment closure model shows over-prediction in this portion. To part after smooth turn, the numerical results gained from Case 2 shows good agreement with experiment.

To side surface, there is big difference between experiment data and numerical result. Numerical results show very low values part before smooth turn, where strong reverse flow and low temperature flow occurs (refer to Fig. 4.5 (a) and (b)). After this portion, compared to experiment data, the results from case 1 shows good agreement, the peak value will reach to 3.5 after the exit of smooth turn due to the strong flow attachment occurring on side surface. However, result from Case 2 shows under-prediction by about 50% lower. To inner surface of part before smooth turn, numerical results from Case 1 show good agreement with experiment data, the flow attachment induced by first sharp turn causes high heat transfer in this region. Compared to Case 1 and Case 2, numerical results shows that the addition of vane increases Nusselt number ratio in turn portion and the effect lasts to part after smooth turn, which is different to experiment data.

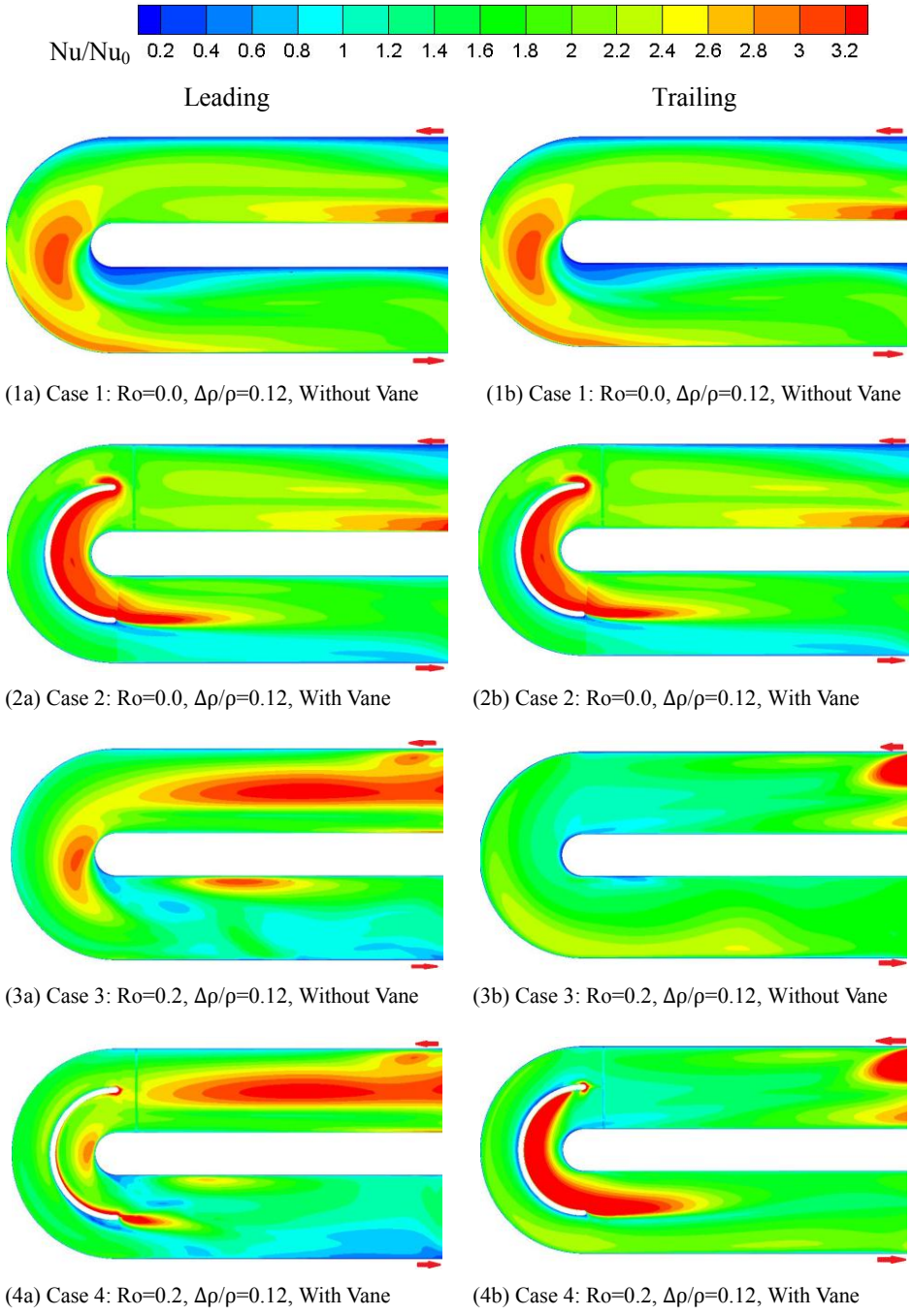

Fig. 4.10 Nusselt number ratio contour on (a) leading surface and (b) trailing surface of non-rotating/rotating cooling channels

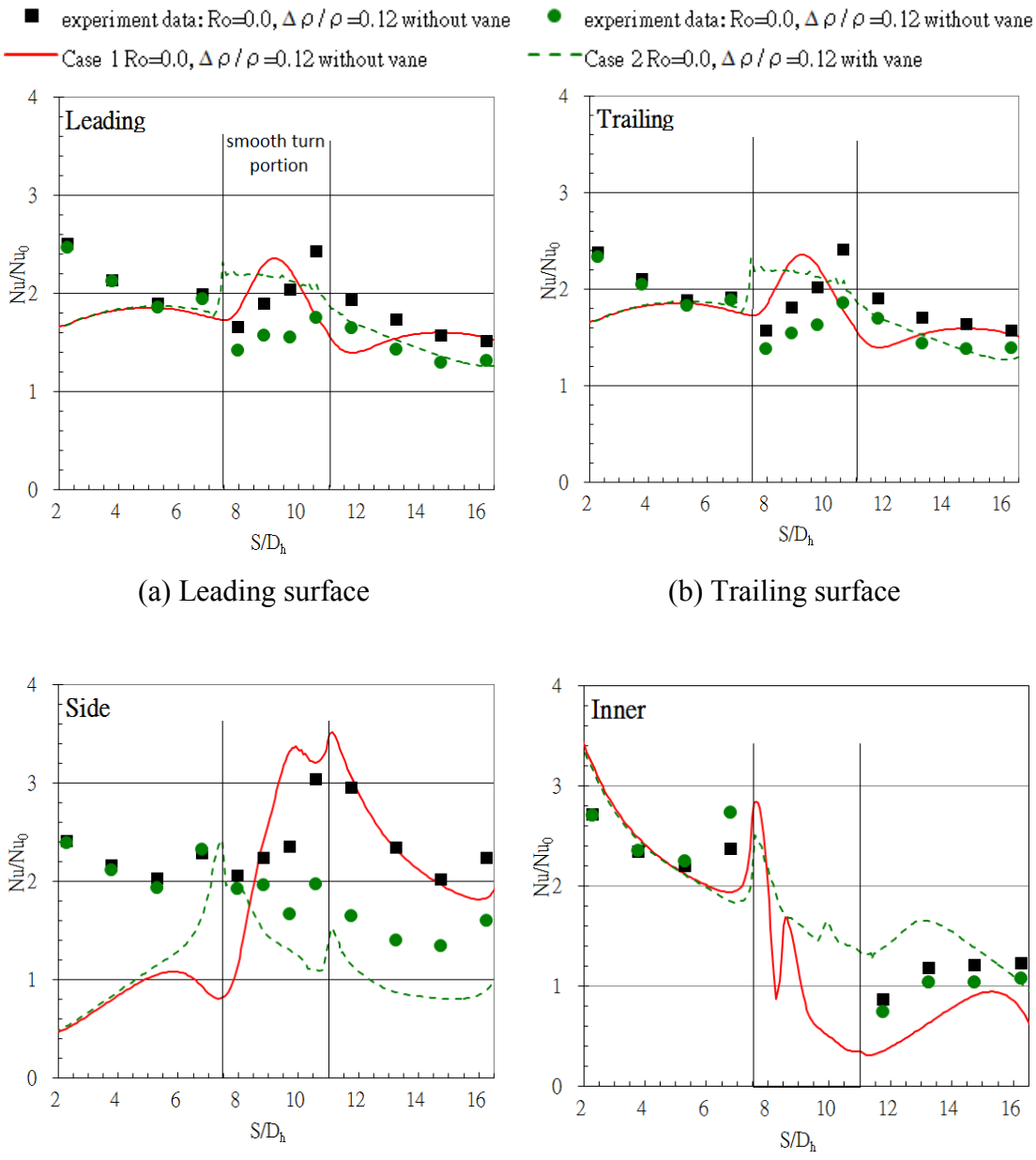

(a) Leading surface

(b) Trailing surface

(c) Side surface

(d) Inner surface

Fig. 4.11 Effect of vane on spanwise-averaged Nusselt number ratio for non-rotating channels

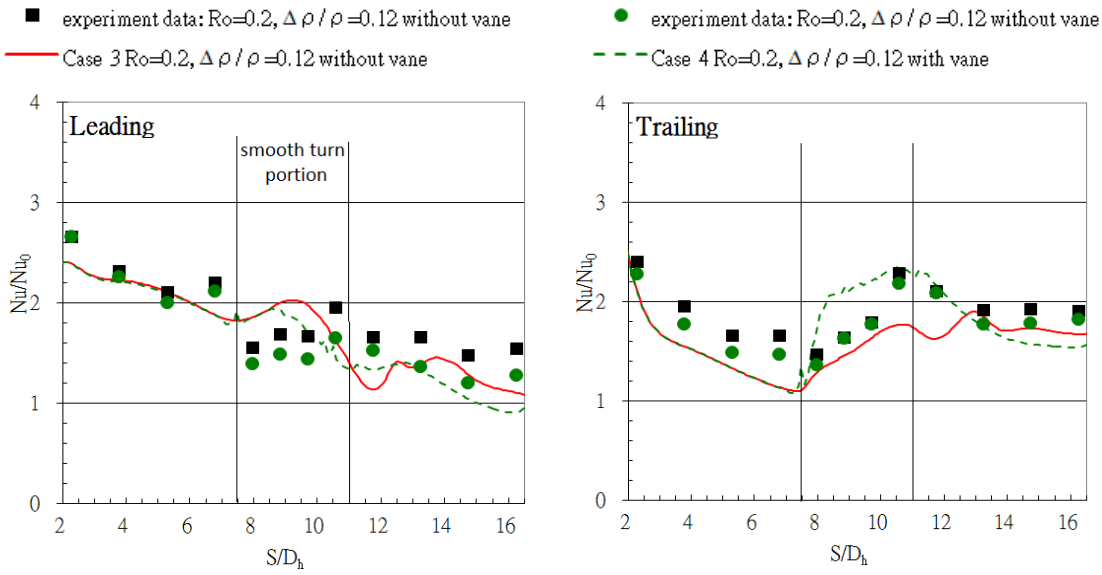

(a) Leading surface

(b) Trailing surface

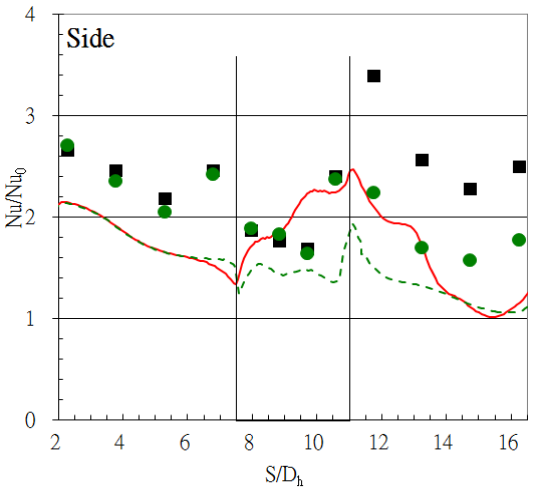

(c) Side surface

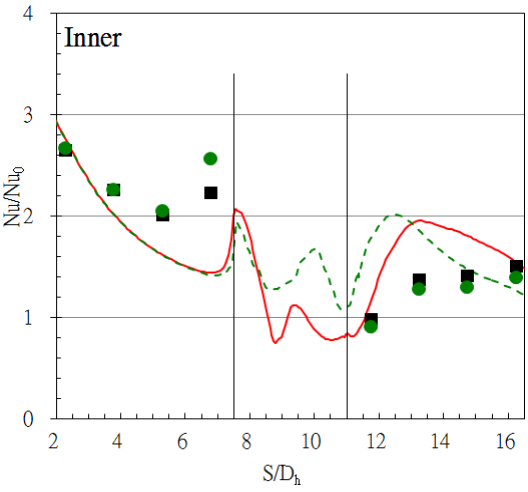

(d) Inner surface

Fig. 4.12 Effect of vane on spanwise-averaged Nusselt number ratio for rotating channels

Fig. 4.12 is the spanwise-averaged Nusselt number ratio for rotating channel. Compared to results from Case 1 and Case 3, in part before smooth turn, it is clear to see that rotation increases Nusselt number ratio on leading surface and decrease Nusselt number ratio on trailing surface. Opposite behaviors occurs in part after smooth turn. The big difference between Case 1 and Case 3 is on the side surface of part before smooth turn. Rotation obviously improves heat transfer in this portion, since it causes flow mixing. Compared to results from Cases 1~4, it is clear to see that the addition of vane does not cause significant influence to part before smooth turn, In turn portion and part after turn, difference between Case 3 and Case 4 is smaller than difference between Case 1 and Case 2. It means vane effect will be decreased by the increase of rotation. This is similar to experiment data.

4.6.1 Effect of Inlet

From chapter 3, it can be concluded that different inlet settings cause significant influence to first passages of four-pass cooling channel. The inlet used in this chapter is circular pipe, which is partially connected to main flowing channel. Fig. 4.13 is the velocity magnitude contour at the center portion of flowing channel. Velocity magnitude used in this figure is calculated from:

$$V_{mag} = \sqrt{U^2 + V^2 + W^2} \tag{4-1}$$

It shows that this set causes stronger inlet cooling. In order to investigate this inlet effect, four-pass channels used in chapter 3 are used here to do comparison. Table 4.3 is the summary of these additional cases.

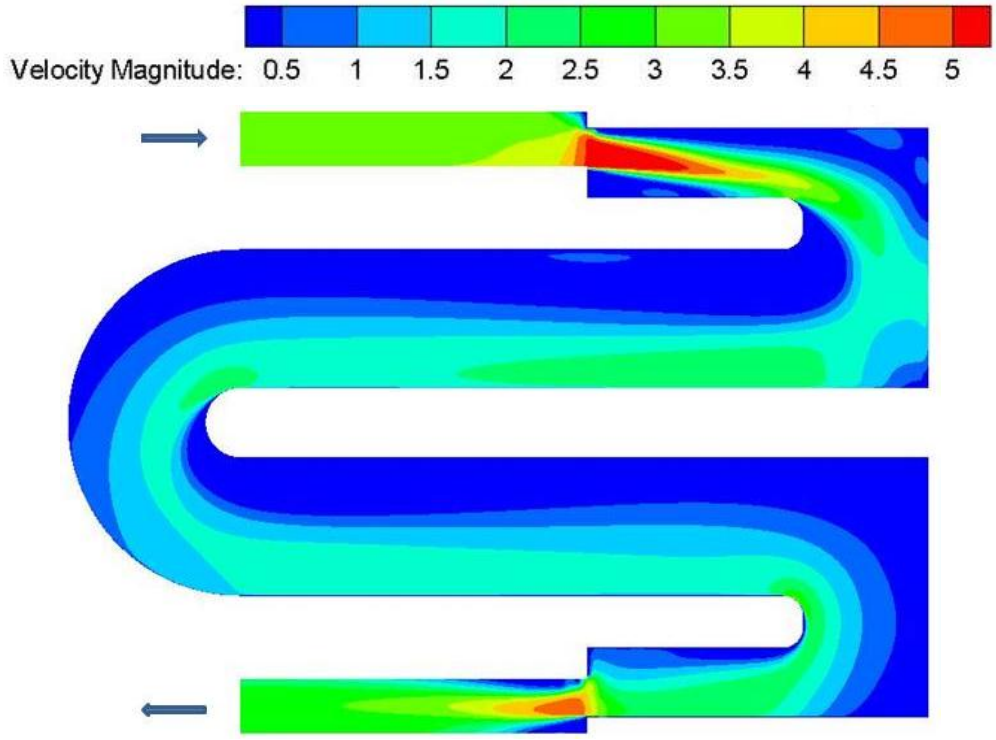

Fig. 4.13 Velocity magnitude at center portion of whole flowing channel under non-rotating condition

Case No.	Re	$\Delta\rho/\rho$	Ro	β	With or without vane
13	20,000	0.12	0.0	-	Four-pass, aspect ratio of whole flowing channel is 2:1
14	20,000	0.12	0.0	-.	Four-pass, aspect ratio of first and fourth pass is 1:1

Table 4.3 Additional cases for inlet effect analysis

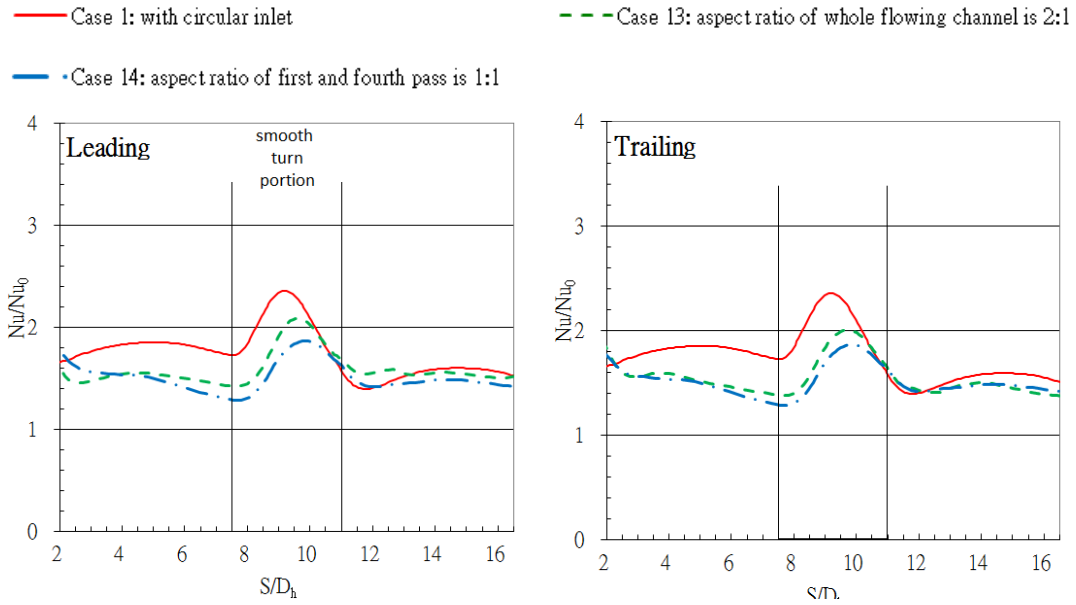

(a) Leading surface

(b) Trailing surface

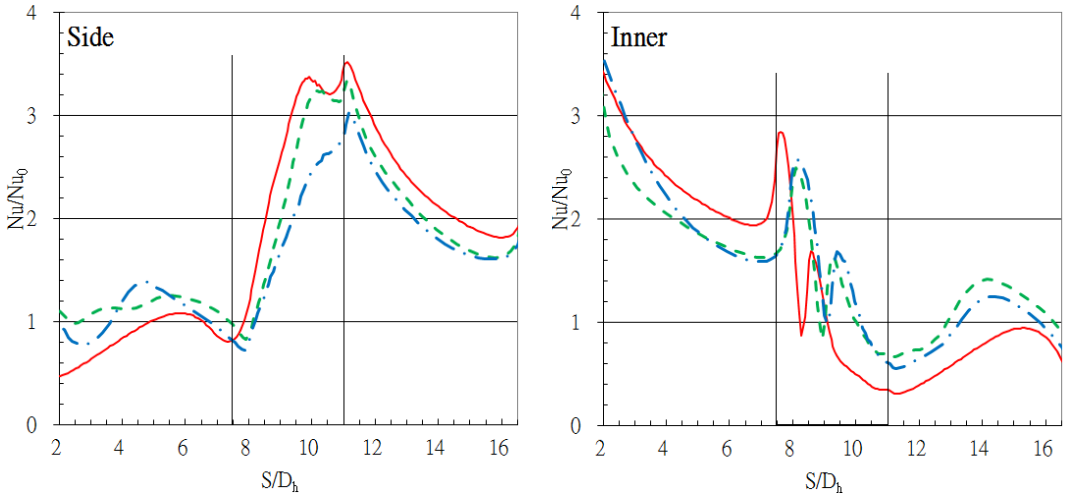

(c) Side surface

(d) Inner surface

Fig. 4.14 Effect of inlet on spanwise-averaged Nusselt number ratio for non-rotating channels

Fig. 4.14 is the spanwise-average Nusselt number ratio for the non-rotating cooling channels with different inlet settings. Among the three geometries, result from Case 1 shows higher Nusselt number ratio on leading and trailing surface. This means this inlet set increases heat transfer on these two faces. This effect lasts to smooth turn portion. Although it raises Nusselt number ratio on leading and trailing surface, it also causes lower Nusselt number ratio on side surface. This is because the strong inlet flow not only impinges outer surface of first sharp turn but also creates big reverse region on inner surface of first sharp turn. This effect lasts to second passage and causes bigger reverse flow region on side surface of second passage.

4.6.2 Effect of Rotation

Fig. 4.15 shows spanwise average Nusselt number ratio for rotating cooling channel without addition of vane. To parts before smooth turn (second passage), main cooling stream flows from tip portion to hub portion, it is radially inward flow. Rotation effect causes heat transfer enhancement on leading surface but decreases heat transfer on trailing surface. To parts after smooth turn, rotation, the flow is radially outward flow, rotation causes opposite effects. Compared to results from non-rotating internal channel (Case 1), with Ro=0.2, Nusselt number ratio on leading surface will be increase by about 20%. With Ro=0.4, Nusselt number ratio on leading surface will be increase by about 40%.

One special thing happens on the trailing surface of part before smooth turn. Nusselt number ratio from Case 5 is higher than Case 3. A slice will be used to explain

this phenomenon. Fig. 4.16 shows location of output slice needed here. Station F is at entrance of first sharp turn. Fig. 4.17 is the velocity magnitude at station F. According to the result, it is clear to see that with higher rotation number, main cooling stream is closer to trailing surface. This is because rotation not only affects flow main flowing channel but also affects flow in inlet circular pipe. With combination of inlet effect and rotation effect, main cooling stream is closer to trailing surface of this portion. According to Fig. 4.15, this effect lasts to second passage and cause higher Nusselt number ratio on trailing surface.

To side surface, the low Nusselt number ratio occurs in part before smooth turn. This is deeply related to reverse flow in this region. However, under rotating condition, rotation effect makes flow mixing. It changes velocity field and temperature distribution in this portion, which also causes heat transfer enhancement and improves Nusselt number ratio in this portion. In smooth turn portion and parts after it, mixing effect induced by rotation also decrease peak value. It makes spanwise-averaged Nusselt number ratio distribution flat.

Fig. 4.18 is the spanwise-average Nusselt number ratio in rotating channel with and without addition of vane. From the figure, it is clear to get the addition of vane does not cause any influence to Nusselt number ratio in part before smooth turn. In turn portion, compared to without vane cases, the addition of vane will cause the trend of Nusselt number flatter and decrease values of Nusselt number ratio. It also can be obtained that the addition of vane decreases difference induced by rotation. In part after smooth turn, the values of Nusselt number ratio will also be affected by the set of vane.

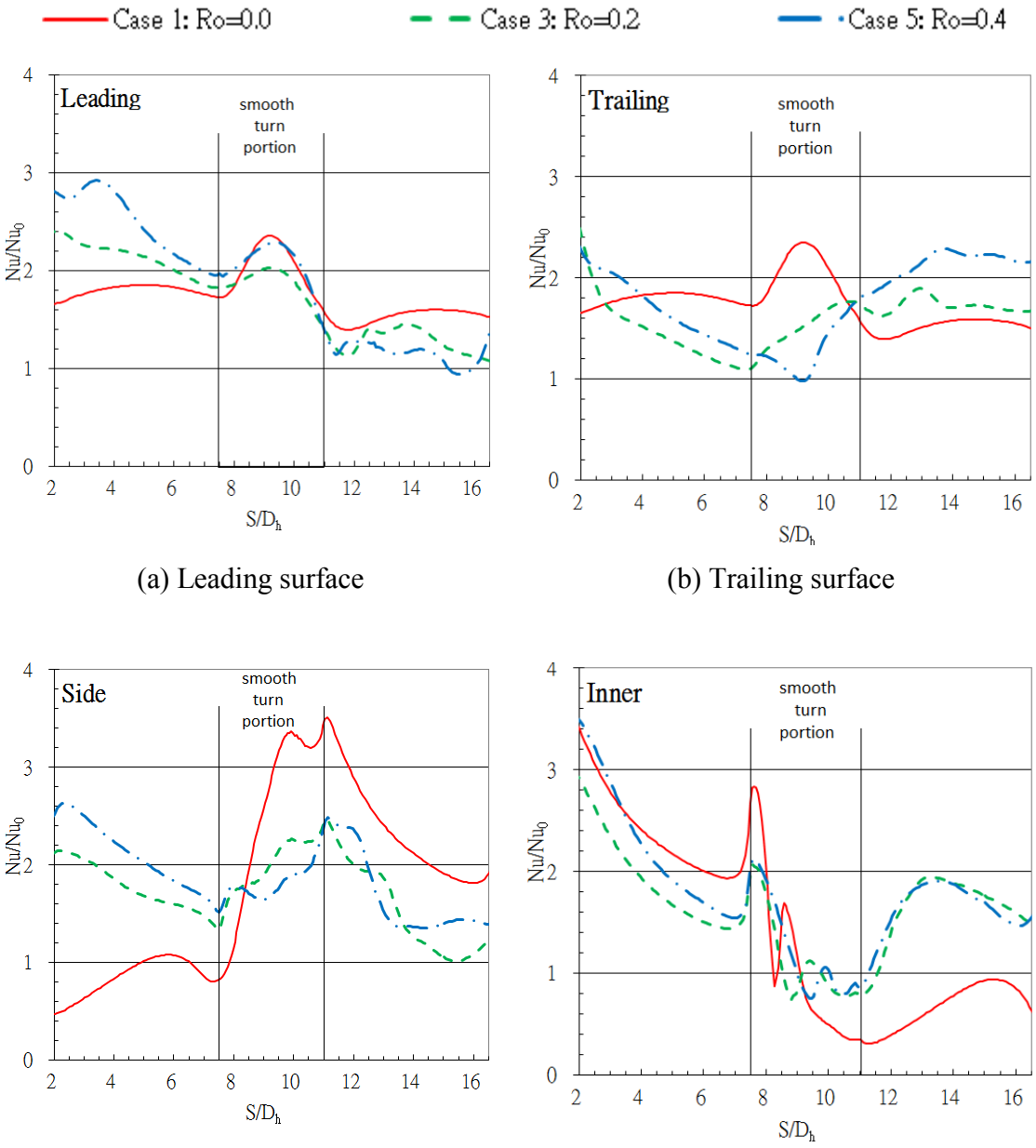

(a) Leading surface

(b) Trailing surface

(c) Side surface

(d) Inner surface

Fig. 4.15 Spanwise-averaged Nusselt number ratio for rotating channel without addition of vane

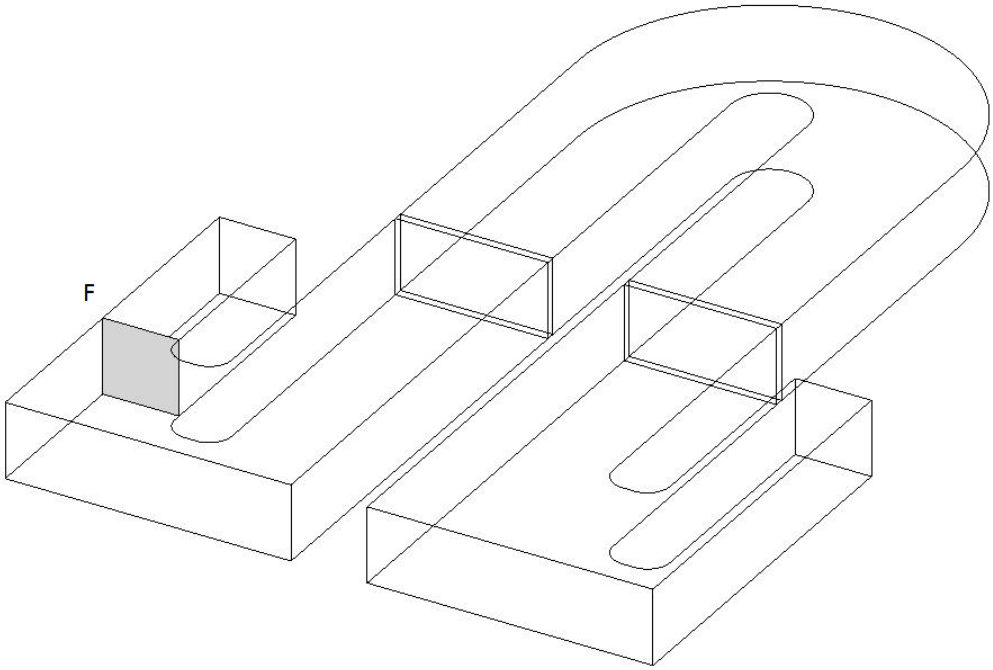

Fig. 4.16 Output slice used for rotation effect

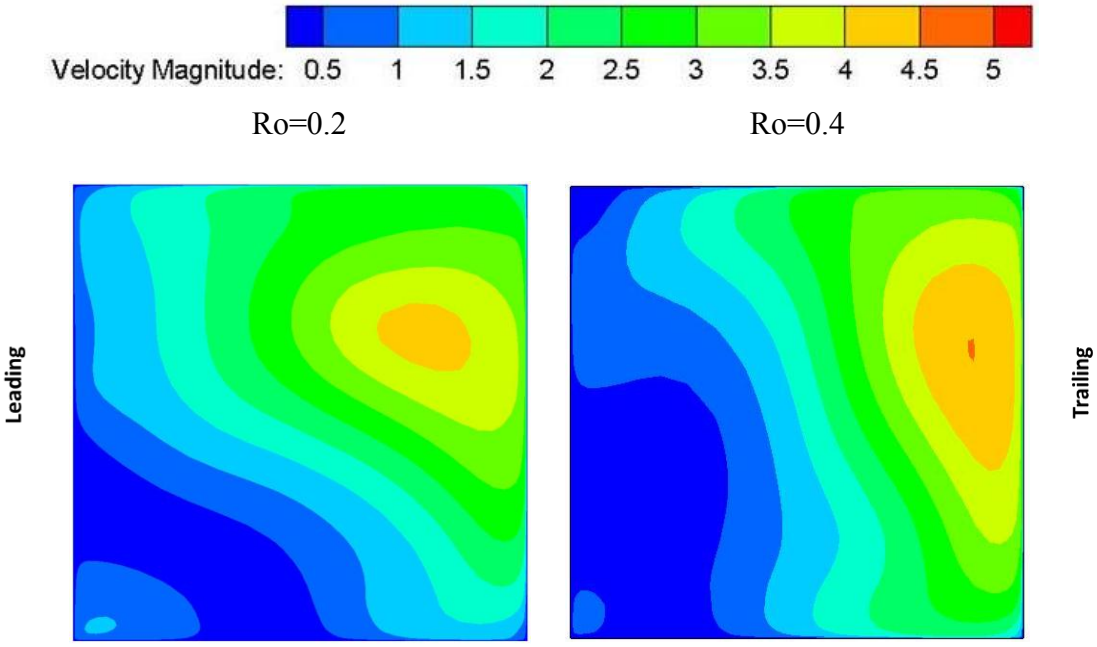

Fig. 4.17 Velocity magnitude of cross section at station F

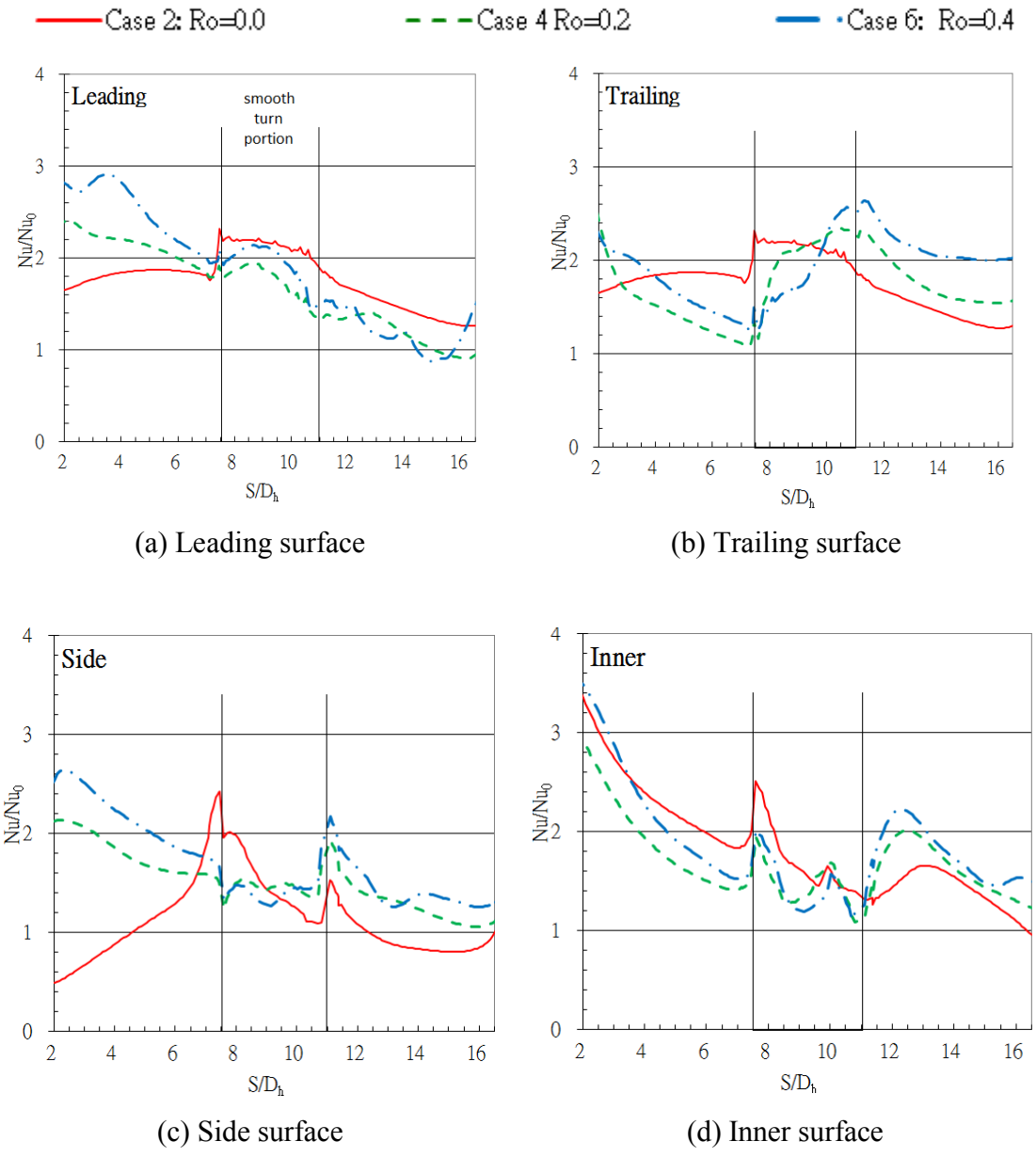

(a) Leading surface

(b) Trailing surface

(c) Side surface

(d) Inner surface

Fig. 4.18 Spanwise-averaged Nusselt number ratio for rotating channels with addition of vane

4.6.3 Effect of Density Ratio

In this part, different density ratio ($\Delta\rho/\rho$=0.12, 0.22, 0.32) will be set to see density ratio effect on heat transfer in a rotating cooling passage (Ro=0.2). Density ratio can be expressed as:

$$\frac{\Delta\rho}{\rho} = \frac{T_W - T_C}{T_W} \tag{4- 2}$$

Tc is inlet coolant temperature. Fig. 4.19 is the spanwised- averaged Nusselt number ratio of Case 3~5. These cases are gained from channels without addition of vane. It can be obtained that density ratio does not cause big influence to part before smooth turn. Even in turn portion and parts after turn, density ratio only causes small influence to Nusselt number ratio.

To this rotating flowing channel, the length of each cooling passage is very short; the cooler stream does not have enough time to react with circumstance. Fig. 4.20 is velocity vector and temperature contour at the center portion of these three cases. No matter in velocity vector or temperature distribution, results from the three cases are almost identical. This causes the results of spanwise averaged Nusselt number ratio from these three cases looks identical in Fig. 4.19

Similar behaviors can be found in cases with addition of vane. Fig. 4.21 is used to evaluate whether density ratio causes influence to spanwise-averaged Nusselt number ratio. To parts before smooth turn, different density ratio does not cause any significant influence to Nusselt number ratio. Only to turn portion and parts after turn, it shows slightly difference.

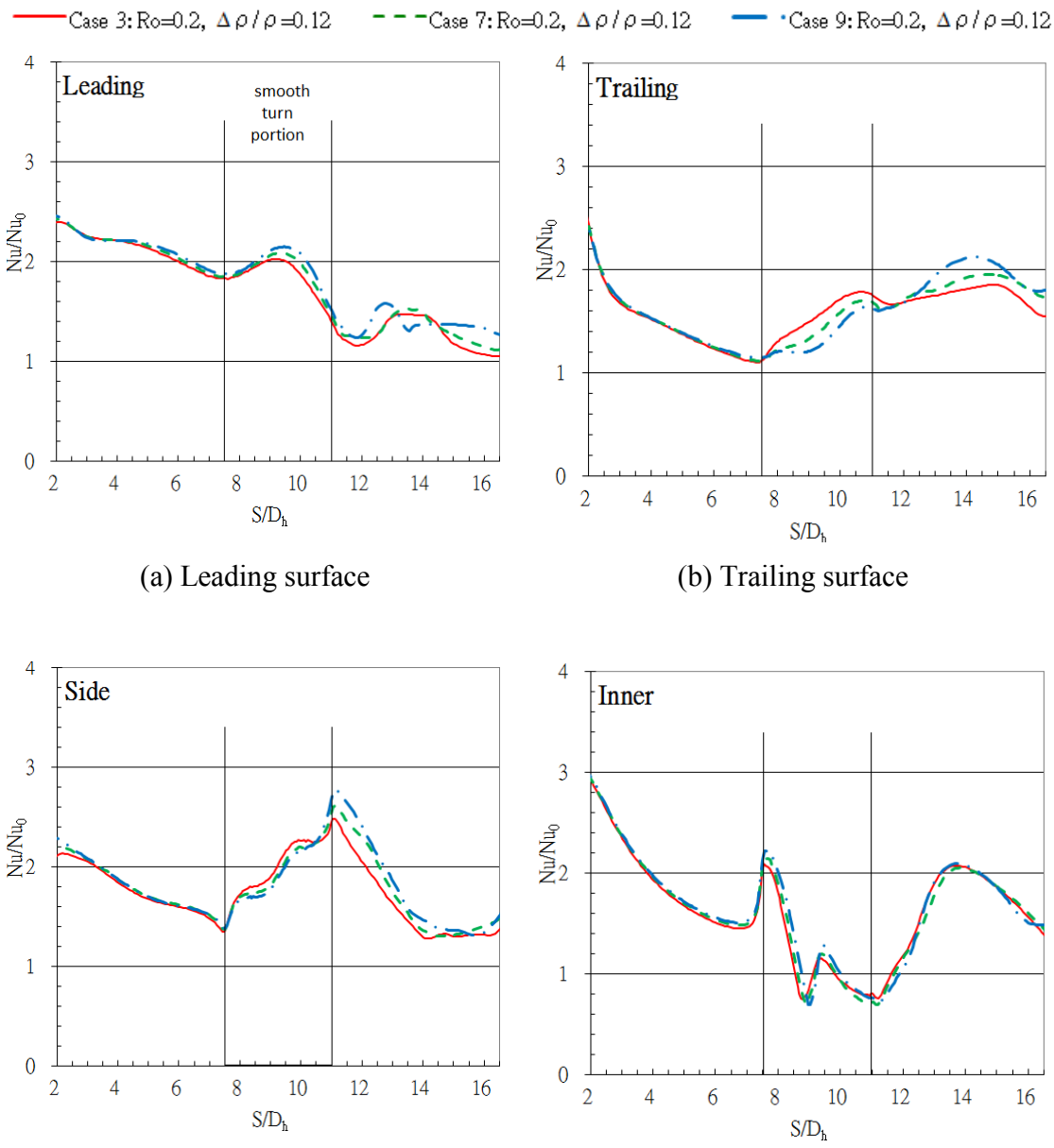

(a) Leading surface

(b) Trailing surface

(c) Side surface

(d) Inner surface

Fig. 4.19 Density ratio effect on spanwise-averaged Nusselt number ratio for rotating channels without addition of vane

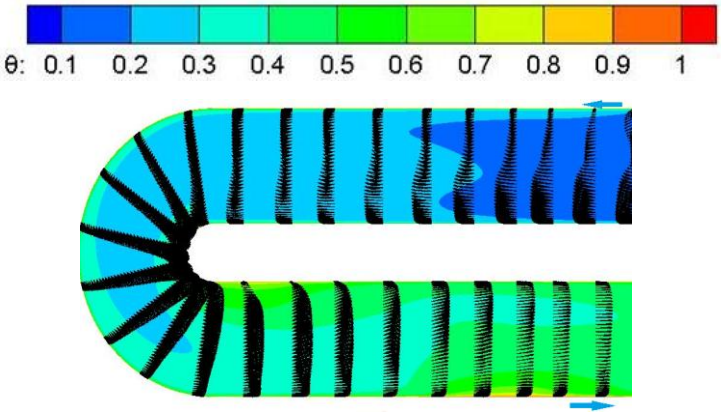

(a) Case 3: Ro=0.2, Δρ/ρ=0.12, Without Vane

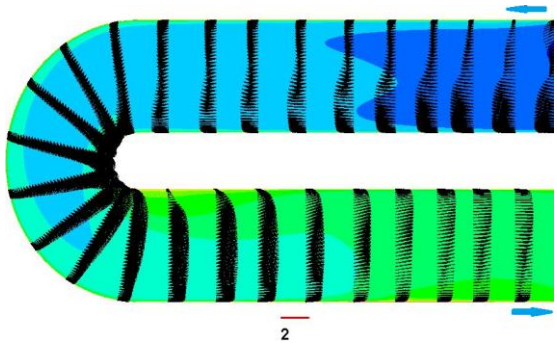

(b) Case 7 : Ro=0.7, Δρ/ρ=0.22, Without Vane

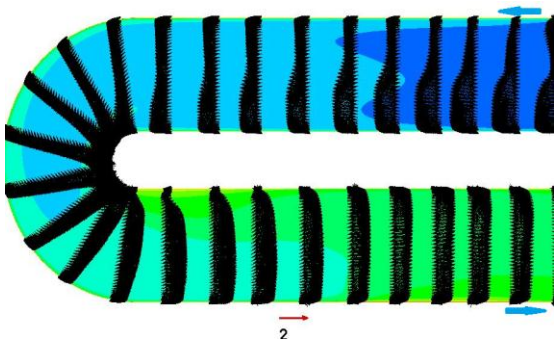

(c) Case 9: Ro=0.2, Δρ/ρ=0.12, Without Vane

Fig. 4.20 Velocity and temperature distribution at the center portion of case 3, 7, 9

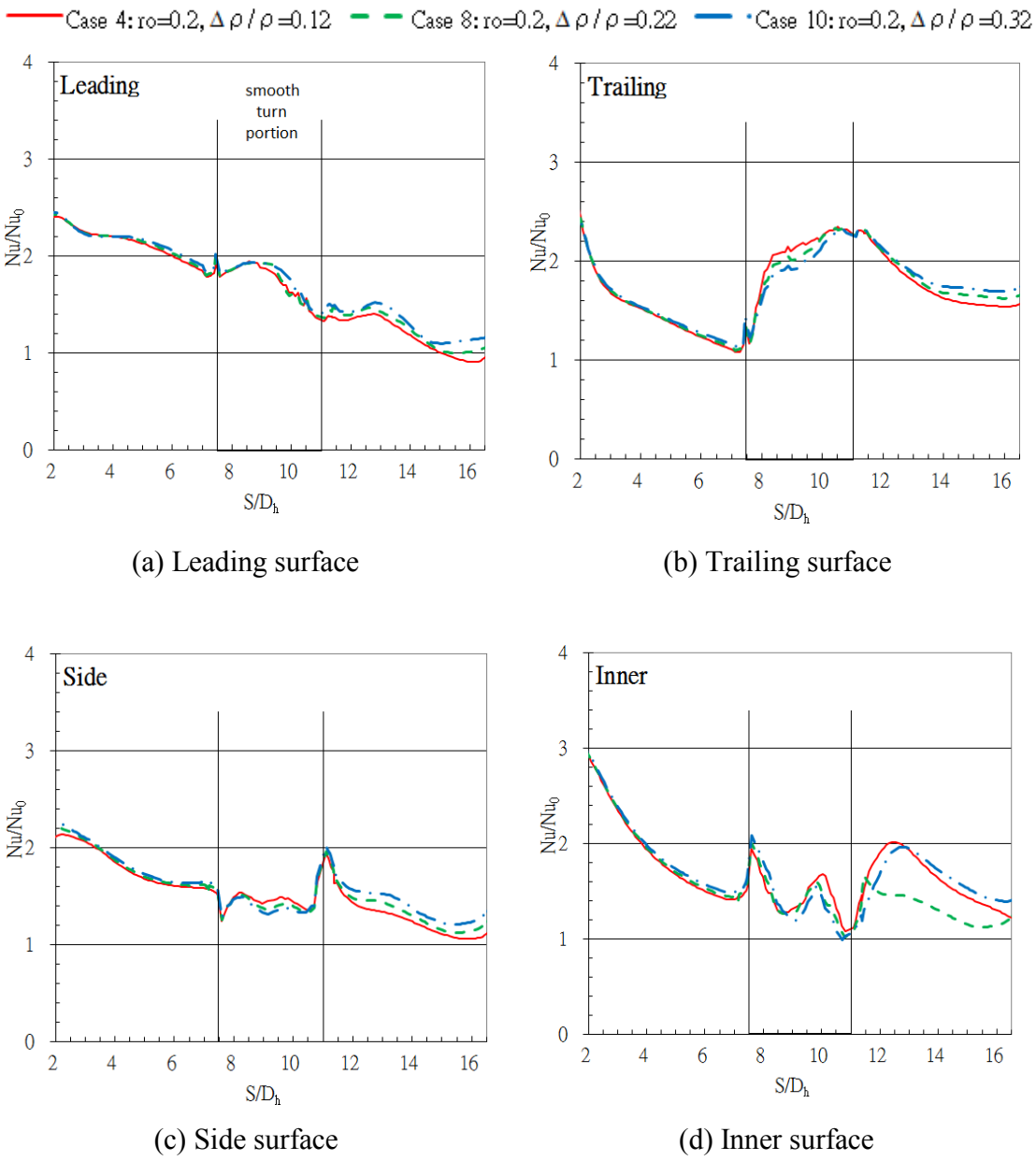

(a) Leading surface

(b) Trailing surface

(c) Side surface

(d) Inner surface

Fig. 4.21 Density ratio effect on spanwise-averaged Nusselt number ratio for rotating channels with addition of vane

4.6.4 Effect of Rotating Angle

Fig. 4.22 is the spanwise-averaged Nusselt number ratio of Case 1,3,11. Generally speaking, in parts before smooth turn, rotation will cause heat transfer enhancement on leading surface but opposite influence on trailing surface. This can be seen in Fig.4.22 (a) and (b). To radially inward flow, the change of rotating angle from 90 degree to 45 degree divides Coriolis force into two minor forces. One still pushes main cooling steam to attach leading surface and the other pushes main cooling stream to side surface.

Fig. 4.23 is secondary flow and temperature distribution for rotating channels with different rotating angle. According to the figure, it can be seen that flow attachment induced by rotation effect decreased with the change of rotating angle.

Fig. 4.24 is the spanwised-averaged Nuseelt number ratio of Case 2,4,12. Compared to Fig. 4.22, it shows the influence resulted from different rotating angle will be decreased by the set of vane.

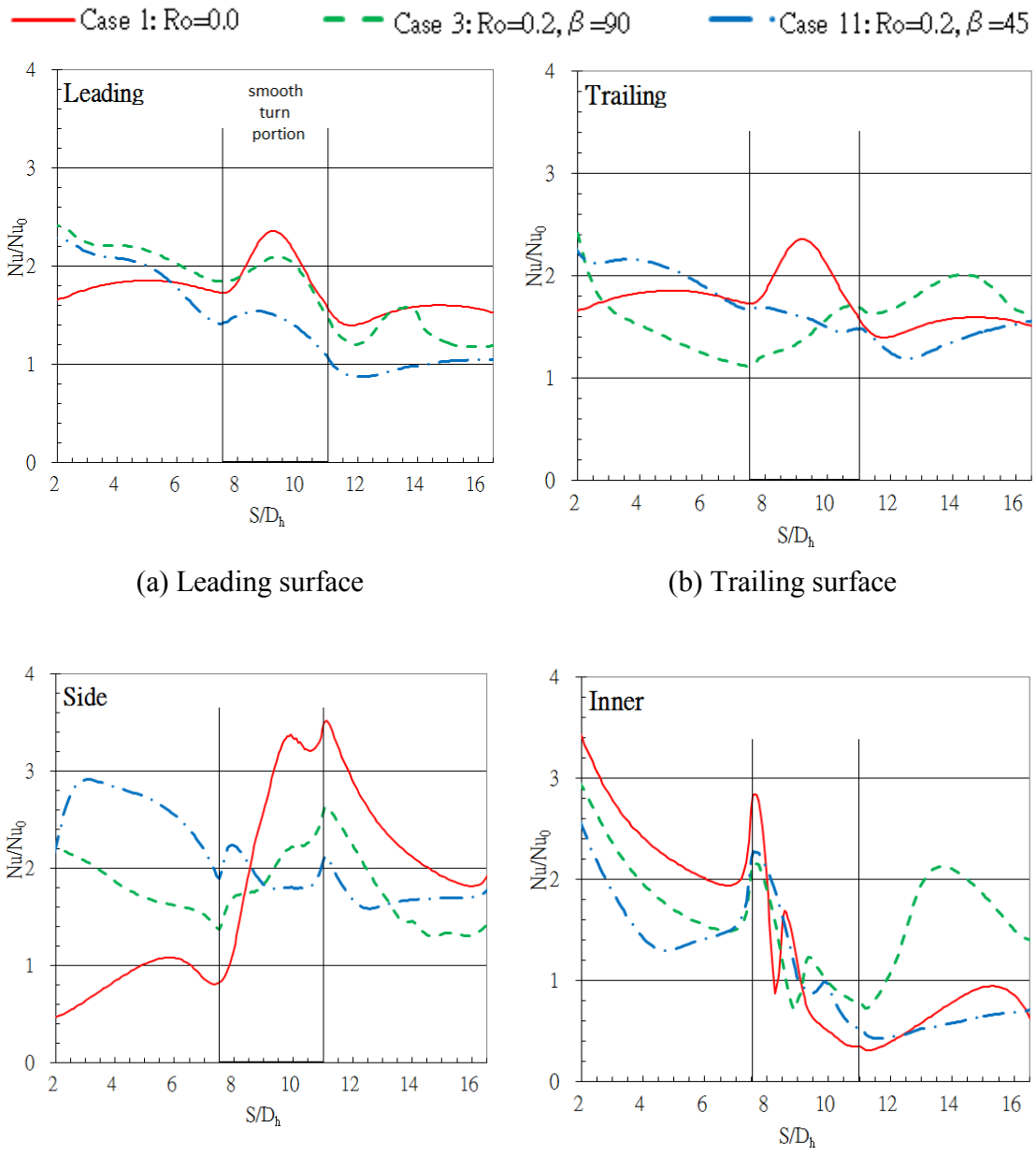

(a) Leading surface

(b) Trailing surface

(c) Side surface

(d) Inner surface

Fig. 4.22 Effect of rotating angle on spanwise-averaged Nusselt number ratio for rotating channels without addition of vane

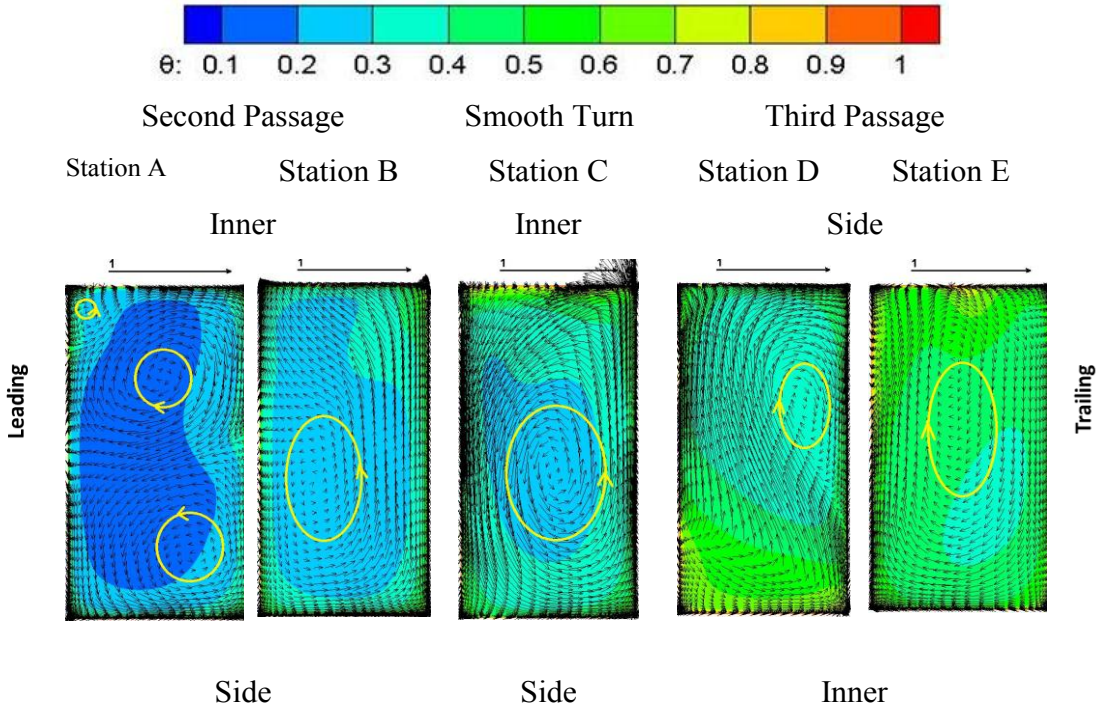

(a) Case 3: Ro=0.2, $\Delta\rho/\rho$=0.12, β=90°, Without Vane

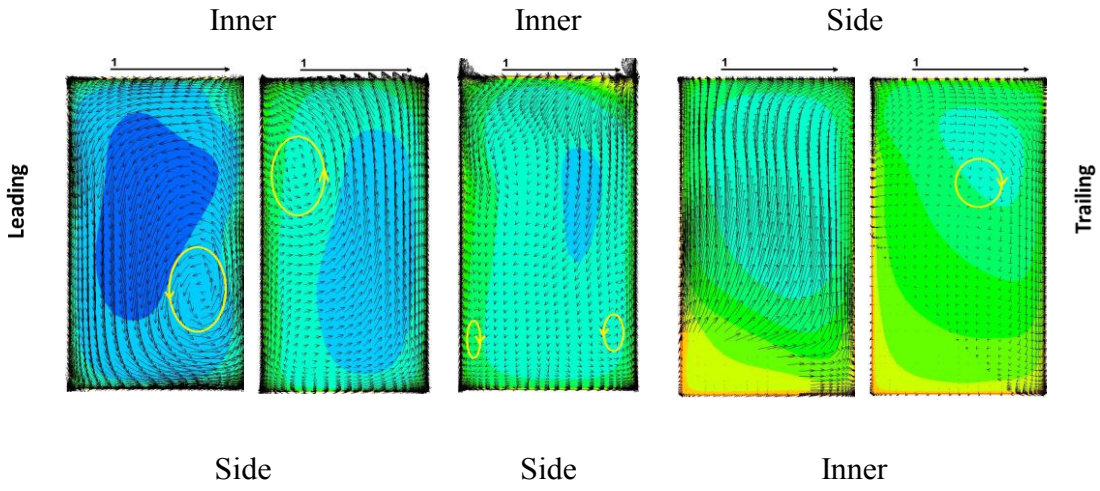

(b) Case 11: Ro=0.2, $\Delta\rho/\rho$=0.12, β=45°, Without Vane

Fig. 4.23 Secondary flow and temperature distribution for rotating channels with different rotating angle

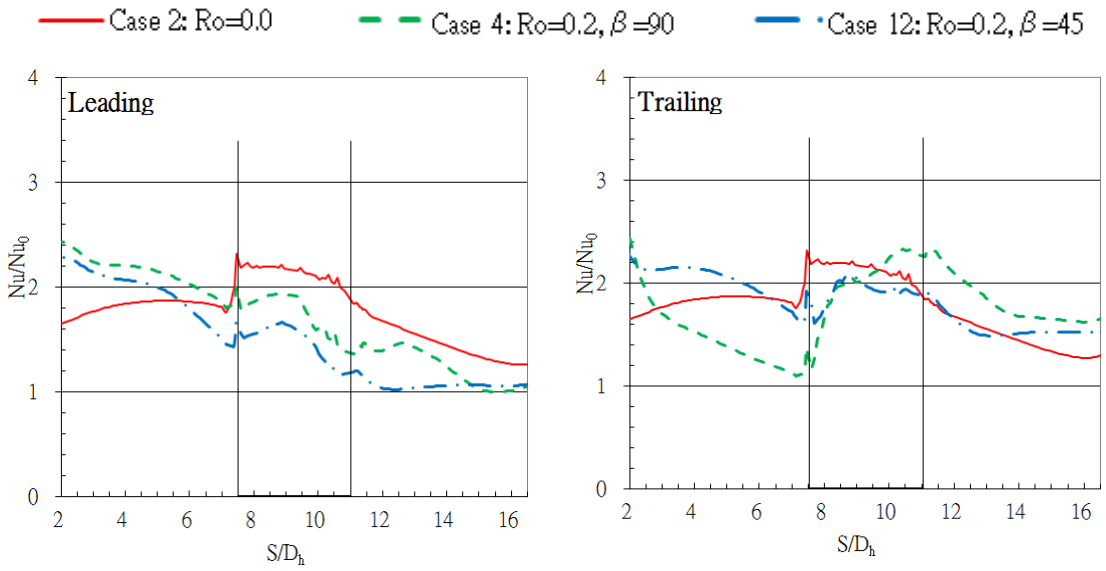

(a) Leading surface

(b) Trailing surface

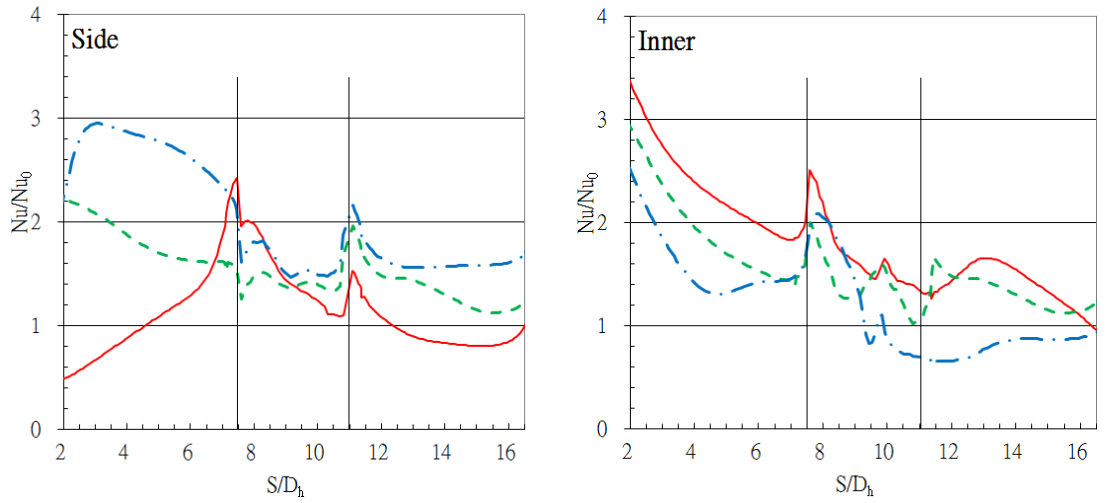

(c) Side surface

(d) Inner surface

Fig. 4.24 Effect of rotating angle on spanwise-averaged Nusselt number ratio for rotating channels with addition of vane

CHAPTER V

CONCLUSION

Second moment closure model was employed to simulate flow and heat transfer in four-pass cooling channel. Several issues can be obtained from the numerical results.

To four-pass channel with different inlet:

1. With same mass flow rate, the decrease of cross-section area in first passage causes stronger inlet flow, which leads to heat transfer enhancement in this region.
2. Stronger inlet flow causes strong impingement on outer surface of first sharp turn and increase heat transfer in this region.
3. Although inlet effect decreases with the increase of distance, it still affects flows and heat transfer in second passage.
4. To parts after second passage, inlet effect does not cause any influence to flow and heat transfer in these regions.
5. To radially inward flow, rotation causes heat transfer enhancement on leading surface and decrease heat transfer on trailing surface. To radially outward flow, rotation shows opposite effect.
6. Inlet effect decrease rotation effect.

To four-pass channel with addition of vane in smooth turn portion:

1. The addition of vane does not cause significant influence to flow and heat transfer in part before it
2. When the flowing channel is under non-rotating condition, the addition of vane

divides main cooling stream into two minor cooling streams. Most cooling stream (64%) flows into inner sub-channel and less main cooling stream (36%) flows into outer sub-channel. This causes Nusselt number ratio in inner sub-channel is much higher than it in outer sub-channel.

3. In part after smooth turn, When the flowing channel is under non-rotating condition, the addition of vane vanishes flow attachment resulted from smooth turn. This decreases heat transfer on side surface but increases heat transfer on inner surface.
4. Overall speaking, when the flowing channel is under non-rotating condition, the addition of vane decreases pressure loss and heat transfer in turn portion.
5. When the flowing channel is under rotating condition, main cooling stream equally flows into two sub-channels. This decreases difference between flow in inner sub-channel and it in outer sub-channel.
6. To radially inward flow, rotation effect increases heat transfer on leading surface but decreases heat transfer on trailing surface. To radially outward flow, it causes opposite influence.
7. The addition of vane in turn portion decreases influence from rotation effect in turn portion and part after it.
8. Density ratio does not cause significant influence in this four-pass channel.
9. The change of rotating angle from 90 degree to 45 degree decreases rotation effect on leading surface and trailing surface. However, it increases heat transfer on side surface.
10. Rotating angle effect causes less influence in flowing channel with addition of vane.

REFERENCES

1. Ekkad, S.V., and Han, J.C., "Detailed heat transfer distributions in two-pass square channels with rib turbulators," *Int. J. Heat Mass Transfer*, **Vol. 40**, **No. 11**, pp. 2525-2537, (1997).
2. Liou, T.-M., and Chen, C.C., "Heat transfer in a rotating two-pass smooth passage with 180° rectangular turn," *International Journal of Heat and Mass Transfer*, **Vol. 42**, pp. 231-247, (1999).
3. Luo, J., and Razinsky, E.H., "Analysis of Turbulent Flow in 180 deg Turning Ducts With and Without Guide Vanes," *ASME Paper,* **No.GT2007-28173**, (2007).
4. Zehnder, F., Schuler, M., Weigand, B., Wolfersdorf, J.V., and Neumann, S.O., "The Effect of Turning Vane on Pressure Loss and Heat Transfer of a Ribbed Rectangular Two-Pass Internal Cooling Channel," *ASME Paper,* **No. GT2009-59482**, (2009).
5. Chen, W., Ren, J., and Jiang, H., "Effect of Turning Vane Configuration on Heat Transfer and Pressure Drop in a Ribbed Internal Cooling System," *ASME Paper,* **No.GT2010-22273**, (2010).
6. Wagner, R.E., and Velkoff, H.R., "Measurements of Secondary Flows in a Rotating Duct," *Journal of Engineering for Power*, **Vol. 94**, pp. 261-270, (1972).
7. Dutta, S., and Han, J.C., "Local Heat Transfer in Rotating Smooth and Ribbed Two-Pass Square Channels With Three Channel Orientations," *ASME J. Heat Transfer,* **Vol. 118**, pp. 578-584, (1996).

8. Huh, M., Lei, J., Liu Y.H. and Han J.C., "High Rotation Number Effects on Heat Transfer in a Rectangular (AR=2:1) Two Pass Channel," *ASME Paper,* **No. GT 2009-59421,** (2009).

9. Hwang, J.J. and Lai, D.Y., "Three-Dimensional Mixed Convection in a Rotating Multiple-Pass Square Channel," *Int. J. Heat Mass Transfer*, **Vol. 41**, pp. 979-991, (1998).

10. Saha, A.K., and Acharya, S., "Unsteady RANS Simulation of Turbulent Flow and Heat Transfer in Ribbed Coolant Passages of Different Aspect Ratios," *ASME Paper,* **No. GT2004-53986**, (2004).

11. Chen, H.C., Jang, Y.J., and Han, J.C., "Near-Wall Second Moment Closure for Rotating Multiple-Pass Cooling Channels," *Journal of Thermodynamics and Heat Transfer*, **Vol. 14, No. 2**, pp. 201-209, (2000).

12. Wagner, J.H., Johnson, B.V., and Hajek, T.J., "Heat Transfer in Rotating Serpentine Passages with Smooth Wall," *ASME J. Turbomachinery*, **Vol. 113**, pp. 321-330, (1991).

13. Su, G., Chen, H.C., Han, J.C., and Heidmann, J.D., "Computation of Flow and Heat Transfer in Rotating Two-Pass Rectangular Channels (AR=1:1, 1:2, and 1:4) with Smooth Walls by a Reynolds Stress Turbulence Model," *International Journal of Heat and Mass Transfer*, **Vol. 47**, pp. 5665-5683, (2004).

14. Tyagi, M. and Acharya, S., "Large Eddy Simulation of Flow and Heat Transfer in Rotating Ribbed Duct Flows," *Journal of Heat Transfer*, **Vol. 127**, pp.486-498, (2005).

15. Wagner, J.H., Johnson, B.V., and Hajek, T.J., 1991a, "Heat Transfer in Rotating Passages with Smooth Walls and Radial Outward Flow," *ASME J. Turbomachinery,* **Vol. 113**, pp. 42-51, (1991).
16. Chen, H.C., Jang, Y.J., Han, J.C., "Computation of Heat Transfer in Rotating Two-Pass Square Channels by a Second-Moment Closure Model," International *Journal of Heat and Mass Transfer*, **Vol. 43**, pp. 1603-1616, (2000).
17. Wright, L.M., Fu, W.L., and Han, J.C., "Influence of Entrance Geometry on Heat Transfer in Rotating Rectangular Cooling Channels (AR=4:1) with Angled Ribs," *ASME J. Heat Transfer*, **Vol. 127**, pp. 378-387, (2005).
18. Lei, J., Li, S.J., Han, J.C., Zhang, L., and Moon, H.K., "Heat Transfer in Rotating Multi-Pass Rectangular Smooth Channel with and Without a Turning Vane," *International Journal of Heat and Mass Transfer,* in Proceeding, (2011).
19. Chen, H.C., "Assessment of a Reynolds Stress Closure Model for Appendage- Hull Junction Flows," *Journal of Fluids Engineering,* **Vol. 117**, pp. 557-563, (1995).
20. Chen, H.C., "Submarine Flows Studied by Second-Moment Closure," *Journal of Engineering Mechanics*, **Vol. 121, No. 10**, pp. 1136-1146, (1995).
21. Chen, H.C, and Patel, V.C., "Near-Wall Turbulence Models for Complex Flows Including Separation," *AIAA Journal*, **Vol. 26, No. 6**, pp. 641-648, (1988).
22. Chen, H.C., Patel, V.C., and Ju, S., "Solutions of Reynolds-Averaged Navier-Stokes Equations for Three-Dimensional Incompressible Flows," *Journal of Computational Physics*, **Vol. 88**, pp. 305-306, (1990).

23. Banek, J.A., Steger, J.L., and Dougherty, F.C., "A Flexible Grid Embedding Technique with application to the Euler Equations," *AIAA Paper*, **No. 83-1944**, pp. 373-382, (1983).

24. Banek, J.A., Buning, P.G., and Steger, J.L., "A 3-D Chimera Grid Embedding Technique," *AIAA Paper*, **No. 85-1523**, pp. 322-331, (1985).

25. Hubbard, B., and Chen, H.C., "A Chimera Scheme for Incompressible Viscous Flows with Application to Submarine Hydrodynamics," *AIAA Paper*, **No. 94-2210**, pp. 1-9, (1994).

26. Al-Qahtani, M., "Computation of Flow and Heat Transfer in Rotating Rectangular Channels with Angles Rib Turbulators for Gas Turbine Blade," Dissertation for Doctor of Philosophy, (2001).

27. Azad, G.S., Uddin, M.J., Han, J.C., Moon, H.K., and Glezer, B., "Heat Transfer in a Two-Pass Rectangular Channel with 45-deg Angled Rib Turbulators," *Journal of Turbomachinary*, **Vol. 124**, pp. 251-259, (2002).